Design of Joint Source-Channel Codes Based on a Generic Protograph

Jia Zhan and Francis C. M. Lau

arXiv:2205.08121v3 [cs.IT] 18 Oct 2022

Abstract

In this paper, we propose using a generic protograph to design joint source-channel codes (JSCCs). We present a generalized algorithm, called protograph extrinsic information transfer for JSCC algorithm (PEXIT-JSCC algorithm), for analyzing the channel threshold of the proposed JSCC. We also propose a source generic protograph EXIT (SGP-EXIT) algorithm, which is more appropriate than the extended source protograph extrinsic information transfer (ESP-EXIT) algorithm for evaluating the source threshold of a generic protograph. Moreover, a collaborative optimization method based on the SGP-EXIT and PEXIT-JSCC algorithms is proposed to construct generic-protograph JSCCs with good source and channel thresholds. Finally, we construct generic-protograph JSCCs, analyze their decoding thresholds, and compare their theoretical and error performance with JSCC systems based on optimized double-protographs. Results show that our proposed codes can outperform double-protograph-based JSCCs.

Index Terms

Asymptotic weight distribution, double protograph, joint source-channel coding, protograph-based extrinsic information transfer analysis, protograph-based low-density-parity-check codes, generic protograph.

I. Introduction

In a digital communication system, source coding is employed to reduce the redundancy in the original information by compression while channel coding is used to protect the compressed data during transmission by adding redundant information (parity check bits). Traditionally, these two types of coding are studied and optimized separately. In particular, when the code length is very large (approaching infinity), the separate design of source and channel coding can theoretically achieve the optimal error performance over an additive white Gaussian noise (AWGN) channel according to the Shannon information theory [2]. However, most real application scenarios cannot afford very long code lengths. They require low encoding/decoding latency and hence prefer short to moderate code lengths. With the recent development of Internet of Things, there has been a growing interest in combining source coding and channel coding with an aim to simplifying the system and/or further optimizing the transmission efficiency and effectiveness.

Part of the paper has been presented in ISTC 2021 [1].

The authors are with the Future Wireless Networks and IoT Focusing Area, Department of Electronic and Information Engineering, The Hong Kong Polytechnic University, Hong Kong SAR. (Emails: jia1206.zhan@connect.polyu.hk and francis-cm.lau@polyu.edu.hk.)

The work described in this paper was supported by a grant from the RGC of the Hong Kong SAR, China (Project No. PolyU 152170/18E).

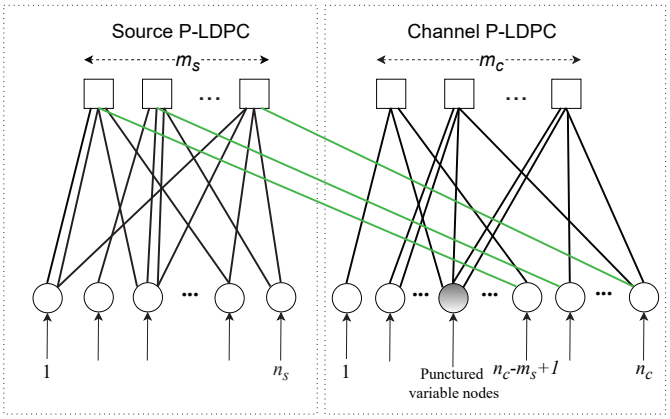


Fig. 1. The protograph representation of a JSCC system in which two P-LDPC codes are cascaded. The source and channel protographs are depicted in the left and right dotted frames, respectively. Variable nodes and check nodes are, respectively, represented by circles and squares; and punctured variable nodes are represented by gray circles. The green solid lines represent the cascading relationship between the source and channel encoders.

The concept of joint source-channel coding (JSCC) was first conceived more than 40 years ago [3]. It has been further investigated since 1990's [4]–[6]. The main idea is to allow the residual redundancy left by the source encoder to be utilized in the tandem joint source-channel decoding algorithms. For example, it is shown that considerable coding gains can be obtained by providing the prior probability of the source bits to the channel decoder [5]. Also when the redundancy of images is utilized in the decoding process, errors can be reduced [7]. In [8], the use of JSCC in JPEG2000 transmission over a two-way relay network is studied; while in [9], [10], the applications of JSCC schemes to wireless video transmissions are investigated. In [11], an iterative joint source-channel decoder is proposed, where messages are exchanged between the decoder of variable length (source) codes (VLC) and the decoder of recursive systematic convolutional codes or low-density parity-check (LDPC) codes. With the use of this iterative joint source-channel decoder, significant error performance gains are observed compared with tandem decoding.

Low-density parity-check (LDPC) codes form a type of capacity-approaching channel codes and have been successfully deployed in many communication systems [12]–[14]. In [15], [16], two LDPC codes are concatenated in series to form a new type of joint source-channel code. Moreover, an iterative decoding algorithm is presented to illustrate the extrinsic information exchange between the source-LDPC decoder and the channel-LDPC decoder.

Protograph LDPC (P-LDPC) codes [17]–[20] are a subset of LDPC codes and they offer fast encoding and decoding structures as well as the linear minimum Hamming distance property. They have been proposed to replace the regular LDPC codes in [16], forming the double protograph-based LDPC JSCC (DP-LDPC JSCC) system [21]. The protograph representation of this JSCC scheme is shown in Fig. 1. Variable nodes and check nodes are represented by circles and squares, respectively; and gray circles denote punctured variable nodes (VNs). The source and channel protographs are shown in the left and right dotted frames, respectively. Firstly, the source symbols are compressed based on the source (left) protograph. Then, the compressed symbols are regarded as the inputs to the channel encoder. The solid green lines, which connect check nodes (CNs) in the source protograph and VNs in the channel protograph in a one-to-one manner, reflecting the cascading relationship between the source encoder and the channel encoder. Finally, the codeword is generated based on the channel (right) protograph.

Fig. 1 can be represented by a joint protomatrix $\mathbf{B}_{J_0}$, i.e.,

$$\mathbf{B}_{J_0} = \begin{pmatrix} \mathbf{B}_s & \mathbf{I}_{m_s}\ \mathbf{0}_{m_s \times m_c} \\ \mathbf{0}_{m_c \times n_s} & \mathbf{B}_c \end{pmatrix} \tag{1}$$

where $\mathbf{B}_s$ indicates the source protomatrix with size $m_s \times n_s$, $\mathbf{B}_c$ indicates the channel protomatrix with size $m_c \times n_c$, $\mathbf{I}_{m_s}$ is an identity matrix of size $m_s \times m_s$, and $\mathbf{0}$ denotes a zero matrix with size indicated by its subscript. Optimizations on the DP-LDPC JSCC system has been performed under different scenarios. In [22] and [23], respectively, an unequal error protection (UEP) technique and an unequal power allocation scheme have been proposed and applied to the DP-LDPC JSCC system. In [24] and [25], the source protomatrix $\mathbf{B}_s$ and the channel protomatrix $\mathbf{B}_c$, respectively, have been redesigned in the JSCC system to improve the error performance. In [26], both source and channel protomatrices are redesigned at the same time to achieve good error-correction capability; while in [27], the optimal distribution of degree-2 VNs in both source and channel protomatrices is studied. In the above studies, error floors are observed at high SNR for DP-LDPC JSCC systems with relatively good performance in the waterfall region.

In [28], it is shown that the aforementioned error floors can be lowered by adding new edges between VNs in the source protograph and CNs in the channel protograph. At the same time, the error performance in the waterfall region will be moderately sacrificed. With the additional edges between VNs in the source protograph and CNs in the channel protograph, Fig. 1 is modified to Fig. 2 and the joint protomatrix in (1) is modified to $\mathbf{B}_J$, i.e.,

$$\mathbf{B}_J = \begin{pmatrix} \mathbf{B}_s & \mathbf{B}_{sccv} \\ \mathbf{B}_{svcc} & \mathbf{B}_c \end{pmatrix} \tag{2}$$

where

$$\mathbf{B}_{sccv} = \begin{pmatrix} \mathbf{I}_{m_s} & \mathbf{0} \end{pmatrix} \tag{3}$$

indicates the source-check-channel-variable linking protomatrix with size $m_s \times n_c$ and $\mathbf{B}_{svcc}$ indicates the source-variable-channel-check linking protomatrix with size $m_c \times n_s$ [29], [30]. Subsequently, the effect of $\mathbf{B}_{svcc}$ on the code performance is studied. In [29], it has been discovered that connecting high-weight columns in $\mathbf{B}_s$ to the rows in $\mathbf{B}_c$ via $\mathbf{B}_{svcc}$ can obtain better error performance. Moreover, if the identity matrix $\mathbf{I}_{m_s}$ in $\mathbf{B}_{sccv}$ is aligned with the high-weight columns in $\mathbf{B}_c$, the error performance can be improved. In other words, CNs in $\mathbf{B}_s$ should be connected to VNs with high degrees in $\mathbf{B}_c$ via $\mathbf{I}_{m_s}$. In [31], several design principles for optimizing $\mathbf{B}_{svcc}$ are proposed to improve the waterfall performance when the source entropy is relatively high. In [32], a search algorithm is proposed to find the best column permutation of $\mathbf{B}_{sccv}$ given $\mathbf{B}_s$ and $\mathbf{B}_c$ are fixed. (Note that permuting the columns of $\mathbf{B}_{sccv}$ while keeping $\mathbf{B}_c$ fixed is equivalent to permuting the columns of $\mathbf{B}_c$ while keeping $\mathbf{B}_{sccv}$ fixed.) In [33], a joint optimization algorithm is provided to construct a joint protograph by taking the error floor and waterfall performance into account at the same time.

Some theoretical analysis tools for the DP-LDPC JSCC system have also been proposed. A joint protograph extrinsic information transfer (JPEXIT) algorithm is proposed in [25] for calculating the channel threshold of the joint protograph shown in Fig. 2. Lowering the channel threshold improves the waterfall performance. To evaluate the error-floor level, we also

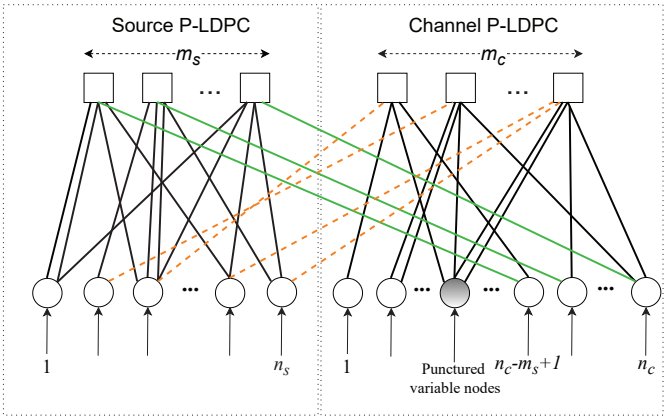


Fig. 2. The protograph representation of the JSCC system where two P-LDPC codes are used and new edges (denoted by orange dashed lines) between variable nodes in the source protograph and check nodes in the channel protograph are added.

need to calculate the source threshold of the double protographs. In [34], a source protograph extrinsic information transfer (SPEXIT) algorithm is proposed to calculate the source thresholds of DP-LDPC codes in the JSCC system when $\mathbf{B}_{svcc}$ is a zero matrix. When $\mathbf{B}_{svcc}$ is a non-zero matrix, a extended source protograph EXIT (ESP-EXIT) algorithm is proposed in [30] to calculate the source thresholds of DP-LDPC codes.

As can be observed, all the aforementioned JSCC systems with DP-LDPC codes have a structural constraint on $\mathbf{B}_{sccv}$, which is shown in (3). In this paper, we remove the above constraint. In other words, $\mathbf{B}_{svcc}$ can be made up of arbitrary non-zero and zero entries. As a result, we view the so-called "joint protomatrix $\mathbf{B}_J$" as a generic protomatrix, and name the corresponding JSCC as "generic protograph-based JSCC (GP-JSCC)" [1]. We consider the performance of the GP-JSCC in both the waterfall region and high signal-to-noise-ratio (SNR) region. Since a lower channel threshold implies a better performance in the waterfall region, we present a protograph EXIT for JSCC (PEXIT-JSCC) algorithm for calculating the channel threshold of a generic P-LDPC (GP-LDPC) code in the JSCC system. It is also known that the source threshold affects the error floor in the high-SNR region. We therefore propose a source generic protograph EXIT (SGP-EXIT) algorithm, which is more generic than the ESP-EXIT algorithm [30], for calculating the source threshold of a GP-LDPC code in the JSCC system. In addition to the source threshold, the linear minimum distance property of a generic protograph can affect the error floor. Given a GP-LDPC code, we will apply the asymptotic weight distribution (AWD) tool [17], [19], [35] to calculate its typical minimum distance ratio (TMDR). If the code has a TMDR, there is a high probability that it possesses the linear minimum distance property, i.e., the minimum distance increases linearly with the codeword length. We illustrate our P-JSCC system by using 'accumulate-repeat-4-jagged-accumulate" (AR4JA) and "accumulate-repeat-3-and-accumulate" (AR3A) codes as examples and forming AR4JA-JSCC and AR3A-JSCC codes [1].

To design a P-JSCC with both good waterfall and error floor performance, we propose a joint optimization method which aims to achieve targeted source threshold and channel threshold. Using AR4JA-JSCC and AR3A-JSCC as benchmarks, we further search for generic protographs in the JSCC schemes using the proposed joint optimization method. Finally, we compare the theoretical (source and channel) thresholds and simulated error performance of the generic protographs found with those of AR4JA-JSCC and AR3A-JSCC. We also compare the results with those from optimized JSCC based on double protographs

in [33].

The main contributions of the paper are as follows.

1) We propose a JSCC scheme based on a generic protograph, namely the "protograph-based JSCC (P-JSCC)".
2) We present a generalized algorithm, namely protograph EXIT for JSCC (PEXIT-JSCC) algorithm for calculating the channel threshold of a GP-LDPC code in the JSCC system.
3) We propose a source generic protograph EXIT (SGP-EXIT) algorithm for evaluating the source threshold of a generic protograph. The proposed technique can be used to calculate the source threshold of a double protograph, and the threshold value obtained is found to be the same as that calculated by the ESP-EXIT algorithm in [30]. The ESP-EXIT algorithm, on the other hand, cannot be utilized to calculate the source threshold of a generic protograph in the JSCC system. Thus the proposed SGP-EXIT algorithm is more generic.
4) We propose a first-source-then-channel-thresholds (FSTCT) joint optimization method based on the SGP-EXIT and PEXIT-JSCC algorithms. The objective is to obtain a generic protograph with a high source threshold and a low channel threshold at the same time. This method is implemented in two steps. The first step is to design a sub-protomatrix (related to the connections between the untransmitted VNs and the connected CNs) in a generic protomatrix to achieve a high source threshold based on the SGP-EXIT algorithm. The second step is to design the remaining part of the generic protomatrix to achieve a low channel threshold based on the PEXIT-JSCC algorithm. Finally, we need to use the asymptotic weight distribution (AWD) tool to analyze the linear minimum distance property of the generic protomatrix/protograph.
5) By using the proposed joint optimization method, we construct some generic protomatrices (P-JSCCs). Both theoretical analysis and error simulations reveal they can outperform AR3A-JSCC, AR4JA-JSCC and the optimized double protographs in [33].
6) Based on the simulation results, we have found that the waterfall performance becomes worse as the source entropy increases. Moreover, a generic protograph designed for a given source entropy does not guarantee its optimality for other given source entropies.

We organize this work as follows. Section II shows the details the proposed JSCC based on a generic protograph. In particular, we provide the structure of the P-JSCC, describe its encoding and decoding method, present a PEXIT-JSCC algorithm for analyzing its channel threshold, propose a SGP-EXIT algorithm for evaluating its source threshold, and propose a FSTCT joint optimization method for constructing good P-JSCCs. In Section III, we present some optimized generic protographs and their theoretical thresholds. We further compare their error rate performance with JSCCs based on optimized double protographs with relevant discussions. Finally, we give some concluding remarks and some future directions in Section IV.

II. Proposed JSCC system with a generic protograph

Referring to Fig. 3, we illustrate the system model of the proposed P-JSCC system using a generic protograph that has no structural constraints. As shown in the figure, VNs and CNs are depicted by circles and squares, respectively. Punctured VNs are denoted by gray circles. VNs corresponding to source symbols are denoted by red circles. This generic protograph can

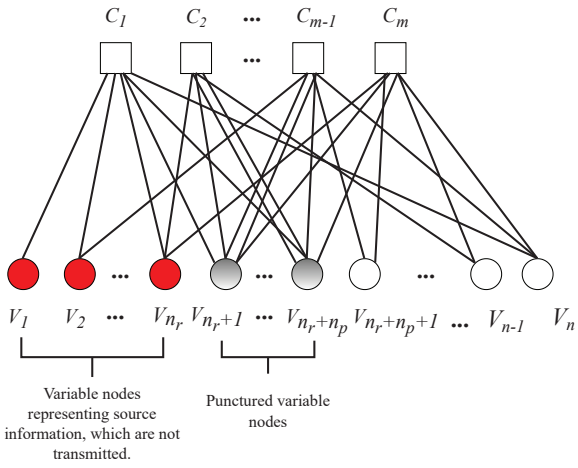


Fig. 3. The proposed P-JSCC system using a generic protograph. Variable nodes and check nodes are, respectively, represented by circles and squares, with gray circles indicating punctured variable nodes and red circles signifying variable nodes corresponding to source symbols.

alternatively be written as a generic protomatrix $\mathbf{B}_{sp}$, i.e.,

$$\mathbf{B}_{sp} = \begin{pmatrix} e_{1,1} & \dots & e_{1,n_r} & \dots & e_{1,n_r+n_p} & \dots & e_{1,n} \\ e_{2,1} & \dots & e_{2,n_r} & \dots & e_{2,n_r+n_p} & \dots & e_{2,n} \\ & & & \vdots & & & \\ e_{m,1} & \dots & e_{m,n_r} & \dots & e_{m,n_r+n_p} & \dots & e_{m,n} \end{pmatrix} \tag{4}$$

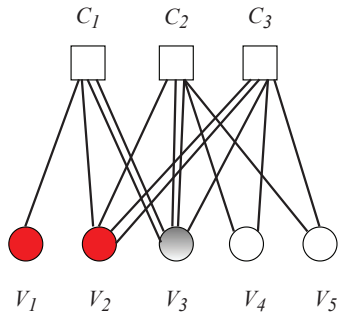
where $e_{i,j}$ denotes the (i,j)-th element ($i = 1, 2, .., m$, $j = 1, 2, ..., n_r, ..., n_r + n_p, ..., n$). Here, m denotes the total number of CNs; n denotes the total number of VNs; n_r denotes the number of VNs corresponding to source symbols; n_p denotes the number of punctured VNs. The overall symbol code rate of the P-JSCC system is given by

$$R = n_r/(n - n_r - n_p). \tag{5}$$

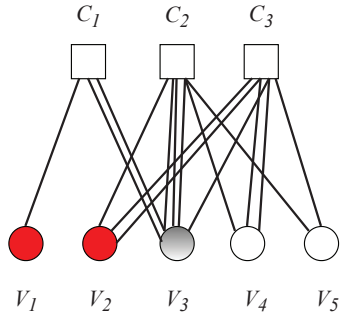
Example: We adopt the conventional AR3A code as our proposed P-JSCC for illustration. Referring to Fig. 4(a), our proposed P-JSCC, namely AR3A-JSCC, consists of

- $m = 3$ CNs (C_1 to C_3);
- $n = 5$ VNs (V_1 to V_5);
- $n_r = 2$ VNs corresponding to source symbols (indicated by red filled circles V_1 and V_2;
- $n_p = 1$ punctured VNs (indicated by the gray circle V_3);
- and an overall symbol code rate $R = 2/(5 - 2 - 1) = 1$.

The corresponding protomatrix of the AR3A-JSCC code is shown in Fig. 5(a) and its size is 3×5. When the conventional AR4JA code is used in our proposed P-JSCC, Fig. 4(b) and Fig. 5(b) show, respectively, the protograph of the AR4JA-JSCC and its corresponding protomatrix.



(a)



(b)

Fig. 4. The protograph of (a) an AR3A-JSCC; (b) an AR4JA-JSCC. Variable nodes and check nodes are, respectively, represented by circles and squares, with gray circles indicating punctured variable nodes and red circles signifying variable nodes corresponding to source symbols.

$$\mathbf{B}_{AR3A-JSCC} = \begin{array}{c} \\ C_1 \\ C_2 \\ C_3 \end{array} \begin{array}{c} \begin{array}{ccccc} V_1 & V_2 & V_3 & V_4 & V_5 \end{array} \\ \begin{pmatrix} 1 & 1 & 2 & 0 & 0 \\ 0 & 1 & 2 & 1 & 1 \\ 0 & 2 & 1 & 1 & 1 \end{pmatrix} \end{array}$$

(a)

$$\mathbf{B}_{AR4JA-JSCC} = \begin{array}{c} \\ C_1 \\ C_2 \\ C_3 \end{array} \begin{array}{c} \begin{array}{ccccc} V_1 & V_2 & V_3 & V_4 & V_5 \end{array} \\ \begin{pmatrix} 1 & 0 & 2 & 0 & 0 \\ 0 & 1 & 3 & 1 & 1 \\ 0 & 2 & 1 & 2 & 1 \end{pmatrix} \end{array}$$

(b)

Fig. 5. The protomatrix of (a) an AR3A-JSCC code; (b) an AR4JA-JSCC code.

A. Encoder

To generate an overall parity-check matrix, $\mathbf{B}_{sp}$ can be lifted by the progressive-edge-growth (PEG) algorithm [36] which can maximize the girth (i.e., smallest cycle) of the resultant Tanner graph. Assume a lifting factor of z, the size of the lifted parity-check matrix, denoted by $\mathbf{H}_{sp}$, equals $mz \times nz$. We assume a binary independent and identically distributed (i.i.d.) Bernoulli source. Denoting the probability of "1" in the source sequence by p_1, the probability of "0" in the source equals $1 - p_1$. Therefore, the source entropy is given by

$$H_p = -p_1 \log_2 p_1 - (1 - p_1) \log_2 (1 - p_1), \tag{6}$$

where $p_1 \neq 0.5$. For example, when the source probability $p_1 = 0.04$, the source entropy $H_p = 0.242$ bit/symbol.

To begin with, we generate a source sequence with a size of $1 \times n_r z$ where the probability of "1" is p_1. The source is directly

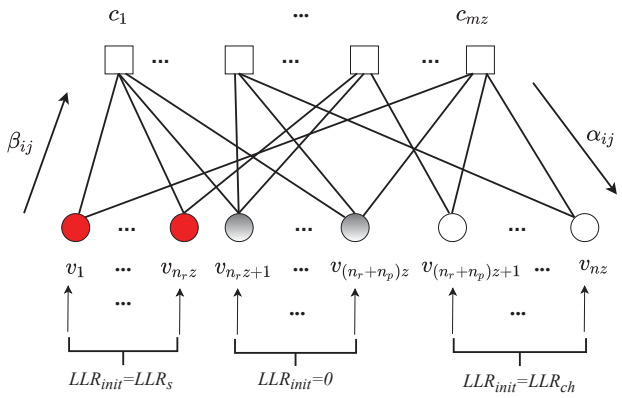


Fig. 6. Decoding of the P-JSCC.

utilized as the input (referred to as v_1 to $v_{n_r z}$ VNs in Fig. 6) to the joint encoder and generate the codeword $(v_1, \ldots, v_{nz})$ based on the parity-check matrix $\mathbf{H}_{sp}$. Finally, the source symbols (v_1 to $v_{n_r z}$) and the punctured bits (i.e., $v_{n_r z+1}$ to $v_{(n_r+n_p)z}$ in Fig. 6) are not transmitted while the code bits $v_{(n_r+n_p)z+1}$ to v_{nz} are sent.

B. Decoder

Fig. 6 illustrates the decoding of the P-JSCC. We define the following.

- $I_{\max}$ is the maximum number of decoding iterations.
- Binary phase-shift-keying modulation is used where bit "1" and "0" are mapped to "-1" and "$+1$", respectively.
- The noise variance of the AWGN channel is given by σ^2.
- The received signal is given by $y = \pm 1 + \eta$ where $\eta \sim N(0, \sigma^2)$ denotes the AWGN.
- M and N, respectively, represent the number of CNs and VNs in the parity-check matrix $\mathbf{H}_{sp}$. They equal mz and nz, respectively, i.e., $M = mz$ and $N = nz$.
- $LLR_{init}(j)$ represents the initial log-likelihood-ratio (LLR) of the j-th VN ($j = 1, 2, ..., N$).
- α_{ij} represents the LLR message sent from the i-th CN to the j-th VN.
- β_{ij} denotes the LLR message sent from the j-th VN to the i-th CN.
- $L_{APP,j}$ denotes the posterior LLR of the j-th VN.
- $\mathcal{M}(j)$ and $\mathcal{N}(i)$ represent the set of all CNs connected to the j-th VN and the set of all VNs connected to the i-th CN, respectively.
- $\mathcal{M}(j)\backslash i$ denotes the set of all CNs connected to the j-th VN excluding the i-th CN; and $\mathcal{N}(i)\backslash j$ denotes the set of all VNs connected to the i-th CN excluding the j-th VN.

The decoding process is described as follows. It is similar to that of decoding a traditional LDPC code except the initialization process.

Initialization:

- Set $\alpha_{ij} = \beta_{ij} = 0 \ \forall i, j$.

- As shown in Fig. 6, LLR_{init} is given by

$$LLR_{init}(j) = \begin{cases} LLR_s(j), & j = 1, 2, ..., n_r z \\ 0, & j = n_r z + 1, n_r z + 2, \\ & ..., (n_r + n_p) z \\ LLR_{ch}(j), & j = (n_r + n_p) z + 1, \\ & (n_r + n_p) z + 2, ..., nz \end{cases} \tag{7}$$

  where $LLR_s(j) = \ln((1-p_1)/p_1)$ represents the initial LLR information of the source symbols; and $LLR_{ch}(j) = 2y_j/\sigma^2$ represents the initial LLR information from the channel.

Iterative process:

- Start: Set the iteration counter $r = 1$.
- Step 1) Updating LLRs from the VNs to the CNs:

$$\beta_{ij} = LLR_{init}(j) + \sum_{i' \in \mathcal{M}(j) \backslash i} \alpha_{i'j}, \ \forall i, j \tag{8}$$

- Step 2) Update LLRs from the CNs to the VNs

$$\alpha_{ij} = 2 \tanh^{-1} \left(\prod_{j' \in \mathcal{N}(i) \backslash j} \tanh(\beta_{ij'}/2) \right), \ \forall i, j. \tag{9}$$

- Step 3) Calculate the posterior LLRs by

$$L_{APP,j} = LLR_{init}(j) + \sum_{i \in \mathcal{M}(j)} \alpha_{ij}, \ \forall j. \tag{10}$$

- Step 4) Estimate v_j by

$$\hat{v}_j = 0 \text{ if } L_{APP,j} \geq 0, \text{ otherwise } \hat{v}_j = 1, \ \forall j. \tag{11}$$

  If $\hat{\boldsymbol{v}} \cdot \mathbf{H}_{sp}^T = \mathbf{0}$ is satisfied where $\hat{\boldsymbol{v}} = \{\hat{v}_1, \hat{v}_2, ..., \hat{v}_{nz}\}$, or $r = I_{max}$, stop the iteration and output $\hat{\boldsymbol{v}}$ as the joint source-channel codeword; otherwise increase the iteration counter r by 1, and repeat Step 1) to Step 4).

C. PEXIT-JSCC algorithm

Denoting E_s as the average transmitted energy per source symbol and N_0 as the noise power spectral density, the AWGN noise variance σ^2 and E_s/N_0 is related by

$$\frac{E_s}{N_0} = 10 \log_{10} \frac{1}{2\sigma^2 R} \text{ dB}. \tag{12}$$

We further define the following.

- $I_{A_VC}(i, j)$ denotes the a priori mutual information (AMI) from the j-th VN to the i-th CN (see Fig. 7).
- $I_{A_CV}(i, j)$ denotes the AMI from the i-th CN to the j-th VN (see Fig. 7).
- $I_{E_CV}(i, j)$ denotes the extrinsic mutual information (EMI) from the i-th CN to the j-th VN.

TABLE I
THE PARAMETER SETTINGS OF THE PEXIT-JSCC AND SGP-EXIT ALGORITHMS

PEXIT-JSCC	Δ	t_{max}	δ
	0.001 dB	200	10^{-6}
SSP-JSCC	$\hat{p}_1$	l_{max}	θ
	0.001	200	10^{-6}

- $I_{E_VC}(i,j)$ denotes the EMI from the j-th VN to i-th CN.
- $I_{APP}(j)$ denotes the mutual information (MI) between the a posterior log-likelihood-ratio (APP-LLR) of the j-th VN and its corresponding symbol.
- $(E_s/N_0)^*$ denotes the channel threshold.
- The mutual information (MI) between the VN V_s corresponding to the source symbol and its corresponding LLR_s is defined by [16]

$$\begin{aligned} &J_{\mathrm{BSC}}(\mu, p_1) \\ &= p_1 \times I(V_s; \omega^{(p_1)}) + (1-p_1) \times I(V_s; \omega^{(1-p_1)}) \end{aligned} \tag{13}$$

  where μ signifies the average LLR value of the VN V_s, $\omega^{(p_1)} \sim N(\mu - LLR_s, 2\mu)$, $\omega^{(1-p_1)} \sim N(\mu + LLR_s, 2\mu)$. $I(a;b)$ denotes the MI between a and b.
- An indicator function $\psi(x)$ is defined as

$$\psi(x) = \begin{cases} 0, & \text{if } x = 0 \\ 1, & \text{otherwise.} \end{cases} \tag{14}$$

In **Algorithm 1**, we present our generalized algorithm, namely protograph EXIT for JSCC algorithm (PEXIT-JSCC algorithm), for analyzing the channel threshold of the proposed P-JSCC. Note that our generalized algorithm is similar to those used in analyzing DP-LDPC codes in the literature, e.g., those in [25]. However, our algorithm is generalized in the sense that the protograph does not need to satisfy any specific constraint, i.e., the requirement given by (3) does not exist. The maximum number of iterations t_{max}, step size Δ, and tolerance value δ used in **Algorithm 1** are listed in Table I. Using the PEXIT-JSCC algorithm, the channel thresholds of AR3A-JSCC and AR4JA-JSCC under $p_1 = 0.04$ are found and listed in Table II.

TABLE II
THE CHANNEL THRESHOLDS AND TMDR VALUES OF DIFFERENT PROTOMATRICES GIVEN $p_1 = 0.04$. THE SHANNON LIMIT IS -7.00 dB

	AR3A-JSCC	AR4JA-JSCC	$\mathbf{B}_{sp_opt1}$	$\mathbf{B}_{sp_opt2}$	$\mathbf{B}_{sp_opt3}$	$\mathbf{B}^{47}_{sp_opt1}$	$\mathbf{B}^{47}_{sp_opt2}$
$(E_s/N_0)^*$ (dB)	-5.918	-5.767	-6.102	-5.810	-5.782	-6.163	-5.909
TMDR value	None	0.017	None	None	0.003	None	0.007

D. SGP-EXIT chart

The algorithms in [30], [34] are not suitable for calculating the source thresholds of the P-JSCC system in Fig. 3. In [34], the SPEXIT algorithm is applied to calculate the source threshold of a double protograph with no connections between VNs in the source P-LDPC code and CNs in the channel P-LDPC code. In [30], the ESP-EXIT algorithm does not consider the case with punctured variable nodes. Also, there is a constraint on the structure of $\mathbf{B}_{svcc}$, i.e., each non-zero column only allows

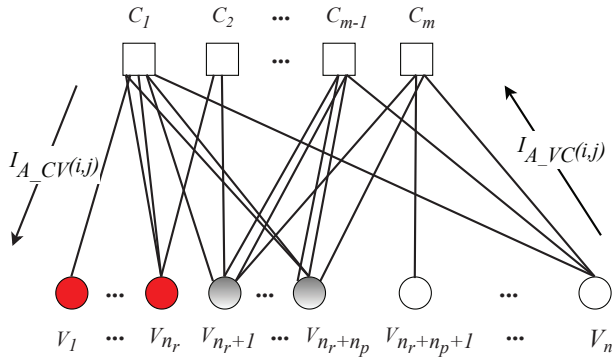
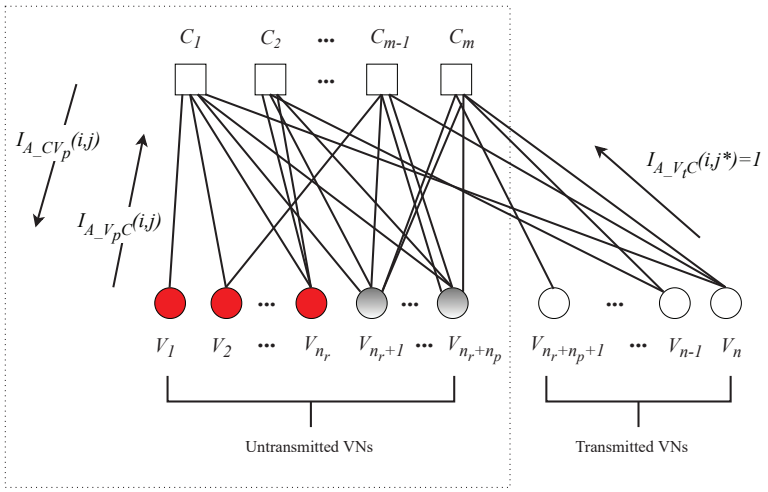


Fig. 7. The protograph of the PEXIT-JSCC algorithm.



(a)

$$\mathbf{B}_{sp} = \left(\begin{array}{ccc|ccc} e_{1,1} & \cdots & e_{1,n_r+n_p} & e_{1,1+n_r+n_p} & \cdots & e_{1,n} \\ e_{2,1} & \cdots & e_{2,n_r+n_p} & e_{2,1+n_r+n_p} & \cdots & e_{2,n} \\ & \vdots & & & \vdots & \\ e_{m,1} & \cdots & e_{2,n_r+n_p} & e_{m,1+n_r+n_p} & \cdots & e_{\mathrm{m},n} \end{array} \right) = (\mathbf{B}_p \mid \mathbf{B}_t)$$

(b)

Fig. 8. (a) Passing of AMI in the protograph representing a P-JSCC. (b) The protomatrix of a P-JSCC is split into two sub-protomatrices. $\mathbf{B}_p$ contains the untransmitted VNs and $\mathbf{B}_t$ contains the transmitted VNs.

a weight of 2. Here, we propose a more generic algorithm for calculating the source threshold of a JSCC system, called the source generic protograph EXIT (SGP-EXIT) algorithm.

First, we refer to Fig. 8(a) and define the following.

- $\mathcal{V}_s = \{V_1, V_2, ..., V_{n_r}\}$ denotes the set of VNs corresponding to source symbols.
- $\mathcal{V}_p = \{V_1, V_2, ..., V_{n_r+n_p}\}$ denotes the set of untransmitted VNs of the generic protograph.
- $\mathcal{V}_t = \{V_{n_r+n_p+1}, V_{n_r+n_p+2}, ..., V_n\}$ denotes the set of transmitted VNs.
- $\mathcal{C} = \{C_1, C_2, ..., C_m\}$ denotes the set of CNs.
- $I_{A_V_pC}(i,j)$ denotes the AMI from the j-th untransmitted VN $\in \mathcal{V}_p$ to the i-th CN.
- $I_{A_V_tC}(i,j^*)$ denotes the AMI from the j^*-th transmitted VN $\in \mathcal{V}_t$ to the i-th CN.
- $I_{A_CV_p}(i,j)$ denotes the AMI from the i-th CN $\in \mathcal{C}$ to the j-th untransmitted VN $\in \mathcal{V}_p$.

Algorithm 1 The PEXIT-JSCC algorithm. The definitions $J(\cdot)$ and $J^{-1}(\cdot)$ are given in [14], [37].

Set the maximum number of iterations t_{max}, step size Δ, and tolerance value δ.
Set a sufficiently small E_s/N_0.
for a given E_s/N_0 **do**
  Set $t=1, I_{E_VC}(i,j)=I_{A_CV}(i,j)=I_{E_CV}(i,j)=I_{A_VC}(i,j)=0$ and $I_{APP}(j)=0, \forall i,j$
  while $\sum_{j=1}^{n}(1-I_{APP}(j))>\delta$ **and** $t \le t_{max}$
    for $i=1,2,..,m$, $j=1,2,..,n$ **do**

$$I_{E_VC}(i,j)=\begin{cases}\psi(e_{i,j})J_{\mathrm{BSC}}\left(\sum_{i'\neq i} e_{i',j}[J^{-1}(I_{A_CV}(i',j))]^2+(e_{i,j}-1)[J^{-1}(I_{A_CV}(i,j))]^2, p_1\right), \\ \qquad\qquad j=1,2,...,n_r \\ \psi(e_{i,j})J\left(\sqrt{\sum_{i'\neq i} e_{i',j}[J^{-1}(I_{A_CV}(i',j))]^2+(e_{i,j}-1)[J^{-1}(I_{A_CV}(i,j))]^2+\sigma_{ch}^2(j)}\right), \\ \qquad\qquad j=n_r+1,n_r+2,...,n\end{cases}$$

where $\sigma_{ch}^2(j)=\begin{cases}0 & j=n_r+1,n_r+2,...n_r+n_p,\\ 4/\sigma^2 & j=n_r+n_p+1,n_r+n_p+2,...,n\end{cases}$

    end for
    Set $I_{A_VC}(i,j)=I_{E_VC}(i,j), \forall i,j$
    for $i=1,2,..,m$, $j=1,2,..,n$ **do**

$$I_{E_CV}(i,j)=\psi(e_{i,j})\left(1-J\left(\sqrt{\sum_{j'\neq j} e_{i,j'}[J^{-1}(1-I_{A_VC}(i,j'))]^2+(e_{i,j}-1)[J^{-1}(1-I_{A_VC}(i,j))]^2}\right)\right)$$

    end for
    Set $I_{A_CV}(i,j)=I_{E_CV}(i,j), \forall i,j$
    for $j=1,2,..,n$ **do**

$$I_{APP}(j)=\begin{cases}J_{\mathrm{BSC}}\left(\sum_{i} e_{i,j}[J^{-1}(I_{A_CV}(i,j))]^2, p_1\right), & j=1,2,...,n_r \\ J\left(\sqrt{\sum_{i} e_{i,j}[J^{-1}(I_{A_CV}(i,j))]^2+\sigma_{ch}^2(j)}\right), & j=n_r+1,n_r+2,...,n\end{cases}$$

where $\sigma_{ch}^2(j)=\begin{cases}0 & j=n_r+1,n_r+2,...n_r+n_p,\\ 4/\sigma^2 & j=n_r+n_p+1,n_r+n_p+2,...,n\end{cases}$

    end for
    Set $t=t+1$
  end while
  if $\sum_{j=1}^{n}(1-I_{APP}(j))<\delta$ **then**
    $(E_s/N_0)^*=E_s/N_0$
    $break$
  else
    $E_s/N_0=E_s/N_0+\Delta$
  end if
end for

- $I_{E_CV_p}(i,j)$ denotes the EMI from the i-th CN $\in \mathcal{C}$ to the j-th untransmitted VN $\in \mathcal{V}_p$.
- $I_{E_V_pC}(i,j)$ denotes the EMI from the j-th untransmitted VN $\in \mathcal{V}_p$ to the i-th CN.
- $I_{APP_}p(j)$ denotes the MI between the APP-LLR of the j-th untransmitted VN $\in \mathcal{V}_p$ and its corresponding symbol.

Next, we can derive the SGP-EXIT curves (i.e., inner-code curve and outer-code curve) of a given P-JSCC using **Algorithm 2**. Note that our objective is to investigate the effect of the source probability p_1 on the source symbol error performance at the high SNR region, i.e., when the noise power is very small. Thus we assume that the average AMI from the transmitted VNs to CNs is equal to 1, i.e., $I_{A_V_tC}(i,j^*)=1$ and $J^{-1}(1-I_{A_V_tC}(i,j^*))=0$ for $i=1,2,...,m, j^*=n_r+n_p+1,n_r+n_p+2,...,n$, and apply it in (17) in **Algorithm 2**. As can be observed in **Algorithm 2** and Fig. 8(a), we only need to consider the

Algorithm 2 Inner-code curve and outer-code curve.

INNER-CODE CURVE

Given $I_{A_CV_p}(i,j) \in [0,1], i = 1,2,...,m, j = 1,2,...,n_r + n_p$

for $i = 1,2,...,m,\ \ j = 1,2,...,n_r$ **do**

$$I_{E_V_pC}(i,j) = \psi(e_{i,j}) J_{\mathrm{BSC}}\left(\sum_{i' \neq i} e_{i',j}[J^{-1}(I_{A_CV_p}(i',j))]^2 + (e_{i,j}-1)[J^{-1}(I_{A_CV_p}(i,j))]^2, p_1\right) \tag{15}$$

end for

for $i = 1,2,...,m,\ \ j = n_r+1, n_r+2, ..., n_r+n_p$ **do**

$$I_{E_V_pC}(i,j) = \psi(e_{i,j}) J\left(\sqrt{\sum_{i' \neq i} e_{i',j}[J^{-1}(I_{A_CV_p}(i',j))]^2 + (e_{i,j}-1)[J^{-1}(I_{A_CV_p}(i,j))]^2}\right) \tag{16}$$

end for

OUTER-CODE CURVE

Given $I_{A_V_pC}(i,j) \in [0,1]$ and $I_{A_V_tC}(i,j^*) = 1, i = 1,2,...,m, j = 1,2,...,n_r+n_p, j^* = n_r+n_p+1,...,n$

for $i = 1,2,...,m,\ \ j = 1,2,...,n_r+n_p$ **do**

$$\begin{aligned} I_{E_CV_p}(i,j) &= \psi(e_{i,j})\left(1 - J\left(\sqrt{\sum_{j' \neq j} e_{i,j'}[J^{-1}(1 - I_{A_V_pC}(i,j'))]^2 + \sum_{j^*=n_r+n_p+1}^{n} e_{i,j^*}[J^{-1}(1 - I_{A_V_tC}(i,j^*))]^2}\right.\right. \\ &\qquad \left.\left. \overline{+(e_{i,j}-1)[J^{-1}(1 - I_{A_V_pC}(i,j))]^2}\right)\right) \\ &= \psi(e_{i,j})\left(1 - J\left(\sqrt{\sum_{j' \neq j} e_{i,j'}[J^{-1}(1 - I_{A_V_pC}(i,j'))]^2 + (e_{i,j}-1)[J^{-1}(1 - I_{A_V_pC}(i,j))]^2}\right)\right) \end{aligned} \tag{17}$$

end for

untransmitted VNs $\mathcal{V}_p$ and their connected CNs in deriving the SGP-EXIT curves. In other words, we only need to consider the sub-protomatrix

$$\mathbf{B}_p = \begin{pmatrix} e_{1,1} & \cdots & e_{1,n_r} & \cdots & e_{1,n_r+n_p} \\ e_{2,1} & \cdots & e_{2,n_r} & \cdots & e_{2,n_r+n_p} \\ & & \vdots & & \\ e_{m,1} & \cdots & e_{m,n_r} & \cdots & e_{m,n_r+n_p} \end{pmatrix} \tag{18}$$

which is also shown in Fig. 8(b).

Considering the protomatrix

$$\mathbf{B}_{sp_opt1} = \begin{pmatrix} 1 & 1 & 1 & 1 & 1 \\ 0 & 0 & 2 & 0 & 1 \\ 3 & 2 & 2 & 0 & 0 \end{pmatrix} \tag{19}$$

and assuming $n_r = 2$ and $n_p = 1$, we form the sub-protomatrix

$$\mathbf{B}_p = \begin{pmatrix} 1 & 1 & 1 \\ 0 & 0 & 2 \\ 3 & 2 & 2 \end{pmatrix} \tag{20}$$

and plot the corresponding SGP-EXIT curves in Fig. 9. We can see that the gap between the inner-coder curve and the outer-

TABLE III
THE SOURCE THRESHOLDS OF DIFFERENT PROTOMATRICES.

	AR3A-JSCC	AR4JA-JSCC	$\mathbf{B}_{sp_opt1}$	$\mathbf{B}_{sp_opt2}$	$\mathbf{B}_{sp_opt3}$	$\mathbf{B}^{47}_{sp_opt1}$	$\mathbf{B}^{47}_{sp_opt2}$
p_{1_th}	0.228	0.212	0.25	0.275	0.242	0.290	0.276

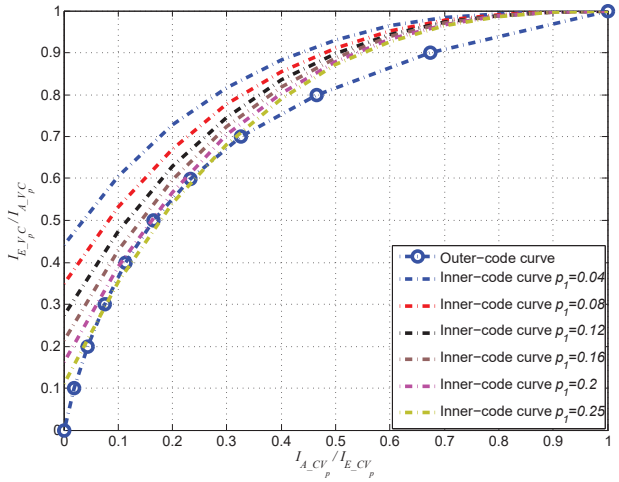


Fig. 9. The SGP-EXIT chart of the sub-protomatrix $\mathbf{B}_p$ in (20) under different p_1 values. Estimated source threshold is 0.25.

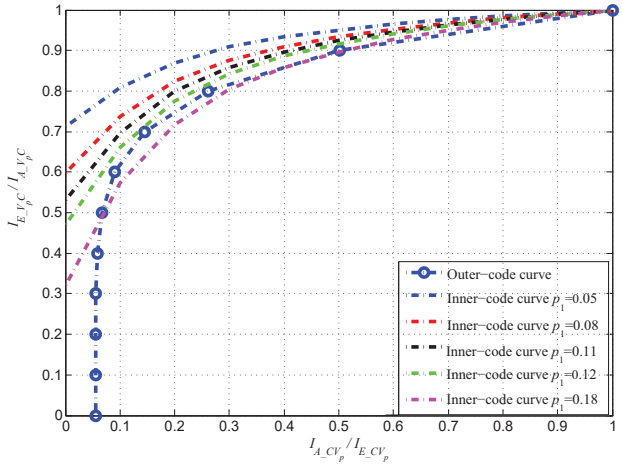


Fig. 10. The SGP-EXIT chart of the sub-protomatrix $\mathbf{B}_p$ in (21) under different p_1 values. Estimated source threshold is 0.12.

code curve becomes smaller as p_1 increases. When p_1 increases beyond a certain value, these two curves will cross each other. The decoding can be performed successfully only when the inner-coder curve is above the outer-coder curve. The larger the gap between the outer-code curve and the inner-code curve, the faster the decoder converges. The maximum p_1 value that makes these two curves closest without crossing is the source threshold p_{1_th}. We can see from Fig. 10 that when $p_1 = 0.25$, the two curves are closest. Then the source threshold of the sub-protomatrix $\mathbf{B}_p$ in (20) is estimated to be $p_{1_th} = 0.25$. To achieve a more precise source threshold, we propose the SGP-EXIT algorithm shown in **Algorithm 3**. The maximum number of iterations l_{max}, step size $\hat{p}_1$ and tolerance value θ used in the algorithm are listed in Table I. Using these parameters, we obtain also $p_{1_th} = 0.25$ for the sub-protomatrix $\mathbf{B}_p$ in (20). Similarly, we apply **Algorithm 3** to obtain the source thresholds of the AR3A-JSCC code and AR4JA-JSCC code in Fig. 5. The source thresholds of the above codes are listed in Table III.

We further consider a DP-LDPC code given by [30, Eq.(26)] where $m = 8, n = 16, n_r = 8, n_p = 0$. Since there is no

Algorithm 3 SGP-EXIT algorithm.

Set the maximum number of iterations l_{max}, step size $\hat{p}_1$ and tolerance value θ.
Set a sufficiently large $p_1 < 0.5$.
for a given $p_1 < 0.5$ **do**
  Set $l = 1, I_{E_V_pC}(i,j) = I_{A_CV_p}(i,j) = I_{E_CV_p}(i,j) = I_{A_V_pC}(i,j) = 0, I_{APP}_p(j) = 0, i = 1,2,..,m, j = 1,2,...,n_r + n_p$.
  while $\sum_{j=1}^{n_r+n_p} (1 - I_{APP}_p(j)) > \theta$ **and** $l \leq l_{max}$
    Compute $I_{E_V_pC}(i,j)$ using (15) and (16) $\forall i,j$.
    Set $I_{A_V_pC}(i,j) = I_{E_V_pC}(i,j)\ \forall i,j$.
    Compute $I_{E_CV_p}(i,j)$ using (17) $\forall i,j$.
    Set $I_{A_CV_p}(i,j) = I_{E_CV_p}(i,j)\ \forall i,j$.
    Calculate $I_{APP}_p(j) = \begin{cases} J_{\mathrm{BSC}}\left(\sum_i e_{i,j}[J^{-1}(I_{A_CV_p}(i,j))]^2, p_1\right), & j = 1,2,...,n_r \\ J\left(\sqrt{\sum_i e_{i,j}[J^{-1}(I_{A_CV_p}(i,j))]^2}\right), & j = n_r+1, n_r+2, ..., n_r+n_p \end{cases}$.
    Set $l = l + 1$.
  end while
  if $\sum_{j=1}^{n_r+n_p} (1 - I_{APP}_p(j)) < \theta$ **then**
    $p_{1_th} = p_1$
    $break$
  else
    $p_1 = p_1 - \hat{p}_1$
  end if
end for

punctured VN, the sub-protomatrix needs to be considered when deriving the source threshold is simply the sub-protomatrix $\begin{pmatrix} \mathbf{B}_s \\ \mathbf{B}_{svcc} \end{pmatrix}$. The sub-protomatrix being studied is given by [30, Eq.(26)]

$$\mathbf{B}_p = \begin{pmatrix} \mathbf{B}_s \\ \mathbf{B}_{svcc} \end{pmatrix} = \begin{pmatrix} 3 & 2 & 1 & 1 & 0 & 1 & 0 & 0 \\ 2 & 3 & 1 & 0 & 1 & 0 & 1 & 0 \\ 3 & 3 & 0 & 0 & 0 & 0 & 0 & 1 \\ 3 & 0 & 1 & 2 & 2 & 1 & 1 & 1 \\ 0 & 0 & 0 & 0 & 0 & 0 & 0 & 0 \\ 0 & 0 & 1 & 0 & 0 & 0 & 0 & 0 \\ 0 & 0 & 0 & 0 & 0 & 0 & 0 & 0 \\ 0 & 0 & 1 & 0 & 0 & 0 & 0 & 0 \end{pmatrix}. \tag{21}$$

Fig. 10 plots the SGP-EXIT chart using **Algorithm 2** under different p_1 values. The estimated source threshold is 0.12. Using **Algorithm 3**, we obtain a more precise threshold, i.e., $p_{1_th} = 0.1156$. This result is the same as that calculated by the ESP-EXIT algorithm in [30].

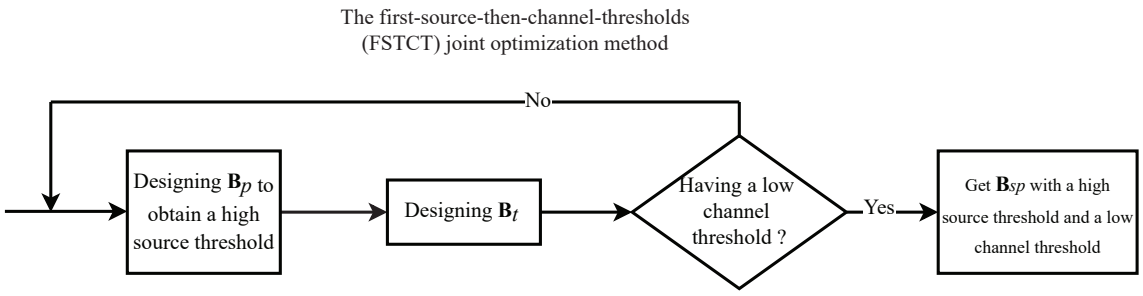


Fig. 11. The flow of the optimization algorithm.

E. Optimization method

We aim to design P-JSCCs with good error performance in both waterfall and high-SNR regions. Our objective is therefore to construct generic protographs with a high p_{1_th} based on the SGP-EXIT algorithm and a low channel decoding threshold $(E_s/N_0)^*$ based on the PEXIT-JSCC algorithm. Moreover, we use the AWD tool to analyze the linear minimum distance properties of the constructed generic protographs.

We propose a first-source-then-channel-thresholds (FSTCT) joint optimization method to design generic protographs. The method is implemented in two steps. The first one is to optimize the connections between the untransmitted VNs and the CNs, i.e., $\mathbf{B}_p$ shown in Fig. 8(b), to obtain a high source threshold (based on the SGP-EXIT algorithm). The second one is to design the remaining part of $\mathbf{B}_{sp}$, i.e., $\mathbf{B}_t$ shown in Fig. 8(b), for a given p_1 to achieve a low channel threshold (based on the PEXIT-JSCC algorithm). The search scope is significantly reduced because $\mathbf{B}_{sp}$ is divided into two parts and are to be optimized one after another. The flow of this method is shown in Fig. 11. By using this optimization method, we can guarantee that the obtained generic protographs have good source and channel thresholds.

As an illustration, we assume a symbol code rate of $R = 1$ and $n_p = 1$ punctured VN. In order to reduce the search space and based on some existing code design rules, we further assume the following conditions.

(i) The maximum value of each entry in $\mathbf{B}_{sp}$ is $e_{max} = 3$.

(ii) The minimum size of the generic protomatrix is 3×5. For $k \in Z^+$, the number of VNs corresponding to source symbols is $n_r = k+1$. According to (5), the total number of VNs is $n = 2k+3$ and the total number of CNs is $m = n-n_r = k+2$.

(iii) The degree of each CN in $\mathbf{B}_{sp}$ is at least 3.

(iv) The maximum number of degree-2 VNs in $\mathbf{B}_{sp}$ is $n - m - n_p = k$.

(v) The maximum number of degree-1 VNs in $\mathbf{B}_{sp}$ is 1 and n_p VNs with the highest degrees in $\mathbf{B}_{sp}$ are punctured.

(vi) The maximum degree of each VN in $\mathbf{B}_{sp}$ is D_{max}. (In this paper, we set $D_{max} = 8$ when $k = 1$; and $D_{max} = 11$ when $k = 2$.)

(vii) $p_{1_th} > \bar{p}_1$ where $\bar{p}_1$ is a preset source threshold benchmark.

(viii) $(E_s/N_0)^* < (E_s/N_0)'$ where $(E_s/N_0)'$ is a preset channel threshold benchmark.

When the search scope is small, a brute-force approach can be used to search for good generic protographs. For example when $k = 1$, the size of $\mathbf{B}_p$ is 3×3 and the size of $\mathbf{B}_t$ is 3×2. In this case, a brute-force search is an option. When the protomatrix is large, the brute-force approach will be very time consuming and even not feasible. Then a differential evolution

(DE) strategy can be used. The following is a more in-depth explanation of these two search methods.

1) Brute-force search: To begin with, we do an exhaustive search for all entries in $\mathbf{B}_p$ that fulfill Conditions (i) to (vii) in accordance with the SGP-EXIT algorithm. Among the $\mathbf{B}_p$'s having high source thresholds, we exhaustively search through all entries in $\mathbf{B}_t$ to make sure $\mathbf{B}_{sp}$ satisfies the conditions (i) to (vi) and (viii) according to the PEXIT-JSCC algorithm.

2) DE approach: We define

- G as the number of generations;
- S as the number of candidate matrices;
- p_c as the crossover probability.

Step a) Initialization: For the 0-th generation, randomly generate candidate matrices $\mathbf{B}^0_{bp_1}, \mathbf{B}^0_{bp_2}, ..., \mathbf{B}^0_{bp_S}$, the size of which equals that of $\mathbf{B}_p$ or $\mathbf{B}_t$, depending on what matrix is to be constructed. Moreover, these matrices should satisfy Conditions (i) to (vi). Set $g = 0$.

Step b) Mutation: Generate S mutation matrices from Generation g using

$$\mathbf{B}^g_{M_s} = \Phi(\mathbf{B}^g_{bp_r1} + 0.5 * (\mathbf{B}^g_{bp_r2} - \mathbf{B}^g_{bp_r3})), \quad s = 1, 2, ..., S \tag{22}$$

where $r1$, $r2$ and $r3$ are distinct random positive integers in the range $[1, S]$, and $\Phi(\cdot)$ is a function that converts each entry in a matrix to an integer closest to its absolute value.

Step c) Crossover: Create the matrix $\mathbf{B}^g_{cr_s}$ $(s = 1, 2, ..., S)$, in which the (i, j)-th element is set as the (i, j)-th element in $\mathbf{B}^g_{M_s}$ with probability p_c, or as the (i, j)-th element in $\mathbf{B}^g_{bp_s}$ with probability $1 - p_c$.

Step d) Selection: Generate the $(g+1)$-th generation candidate matrices $\mathbf{B}^{g+1}_{bp_s}$ $(s = 1, 2, ..., S)$. Two cases are to be discussed.

a) Case One: When the goal is to find a $\mathbf{B}_p$ with a high source threshold, $\mathbf{B}^{g+1}_{bp_s}$ $(s = 1, 2, ..., S)$ is generated as

$$\mathbf{B}^{g+1}_{bp_s} = \begin{cases} \mathbf{B}^g_{cr_s}, & \text{if } \Theta(\mathbf{B}^g_{cr_s})\Psi(\mathbf{B}^g_{cr_s}) > \Theta(\mathbf{B}^g_{bp_s}) \\ \mathbf{B}^g_{bp_s}, & \text{otherwise} \end{cases} \tag{23}$$

where $\Theta(\mathbf{B}_p)$ returns the source threshold p_{1_th} of $\mathbf{B}_p$ according to the SGP-EXIT algorithm; and

$$\Psi(\mathbf{B}^g_{cr_s}) = \begin{cases} 1, & \text{if Conditions (i) to (vi) are} \\ & \text{satisfied by } \mathbf{B}^g_{cr_s} \\ 0, & \text{otherwise.} \end{cases} \tag{24}$$

b) Case Two: When the goal is to find a $\mathbf{B}_t$ such that together with a pre-determined $\mathbf{B}_p$ the generic protomatrix $\mathbf{B}_{sp} = (\mathbf{B}_p\ \mathbf{B}_t)$ can achieve a low channel threshold $(E_s/N_0)^*$, $\mathbf{B}^{g+1}_{bp_s}$ $(s = 1, 2, ..., S)$ is generated as

$$\mathbf{B}^{g+1}_{bp_s} = \begin{cases} \mathbf{B}^g_{cr_s}, & \text{if } \Upsilon\Big((\mathbf{B}_p\ \mathbf{B}^g_{cr_s})\Big)\Psi(\mathbf{B}^g_{cr_s}) \\ & \quad < \Upsilon\Big((\mathbf{B}_p\ \mathbf{B}^g_{bp_s})\Big) \\ \mathbf{B}^g_{bp_s}, & \text{otherwise} \end{cases} \tag{25}$$

where $\Upsilon(\mathbf{B}_{sp})$ returns the channel threshold value of $\mathbf{B}_{sp}$ according to the PEXIT-JSCC algorithm.

Step e) Termination: Set $g = g + 1$. Stop if $g = G$; otherwise go to Step b).

III. Results and discussions

In this section, we present some optimized generic protomatrices, and their theoretical thresholds and error rate simulation results. As discussed in the previous section, the channel thresholds and source thresholds of the AR3A-JSCC and AR4JA-JSCC codes (see Fig. 5) have been derived by the PEXIT-JSCC algorithm under $p_1 = 0.04$ and the SGP-EXIT algorithm, respectively. Referring to Tables II and III, the channel thresholds of AR3A-JSCC and AR4JA-JSCC codes are, respectively, -5.918 dB and -5.767 dB; and the source thresholds are, respectively, 0.228 and 0.212. Based on the results of the AR3A-JSCC and AR4JA-JSCC codes, we construct two sets of benchmarks, i.e.,

- $B_1 : (\bar{p}_1 = 0.228, (E_s/N_0)' = -5.918$ dB); and
- $B_2 : (\bar{p}_1 = 0.212, (E_s/N_0)' = -5.767$ dB).

A. Thresholds of Protomatrices Found

1) Generic protomatrix of size 3×5 and $p_1 = 0.04$: We assume a generic protomatrix of size 3×5 and use the proposed FSTCT joint optimization method under $p_1 = 0.04$ to search for protomatrices with better thresholds than the two sets of benchmarks separately. Since the protomatrix size is relatively small, we apply the brute force searching approach. With B_1 as the benchmark, the proposed FSTCT method finds $\mathbf{B}_{sp_opt1}$ shown in (19) which is repeated below

$$\mathbf{B}_{sp_opt1} = \begin{pmatrix} 1 & 1 & 1 & 1 & 1 \\ 0 & 0 & 2 & 0 & 1 \\ 3 & 2 & 2 & 0 & 0 \end{pmatrix}; \tag{26}$$

and with B_2 as the benchmark, the proposed FSTCT method generates

$$\mathbf{B}_{sp_opt2} = \begin{pmatrix} 3 & 2 & 2 & 0 & 0 \\ 0 & 0 & 3 & 1 & 1 \\ 0 & 1 & 1 & 0 & 1 \end{pmatrix} \tag{27}$$

$$\mathbf{B}_{sp_opt3} = \begin{pmatrix} 1 & 0 & 2 & 0 & 0 \\ 0 & 2 & 3 & 2 & 0 \\ 0 & 1 & 1 & 0 & 3 \end{pmatrix}. \tag{28}$$

The source and channel thresholds of these three codes and AR3A-JSCC and AR4JA-JSCC codes are shown in Table III and Table II, respectively. We can see that these three generic protographs have higher source thresholds than AR3A-JSCC and AR4JA-JSCC codes. (Note that Fig. 9 plots the SGP-EXIT chart of $\mathbf{B}_{sp_opt1}$ under different p_1 values.) In addition, $\mathbf{B}_{sp_opt1}$ has the lowest channel threshold ($(E_s/N_0)^*$=-6.1021 dB) among these five codes, which is about 0.18 dB lower than the decoding threshold of the AR3A-JSCC code. $\mathbf{B}_{sp_opt2}$ and $\mathbf{B}_{sp_opt3}$ have lower channel thresholds compared with the AR4JA-JSCC code.

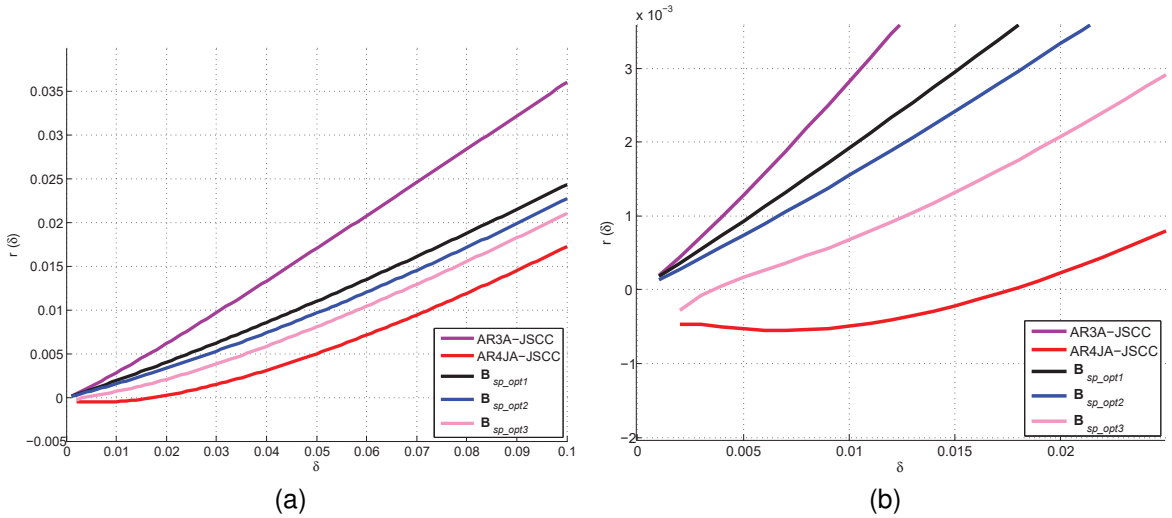


Fig. 12. The asymptotic weight distribution curves of different protomatrices. (a) $\delta \in [0, 0.1]$; (b) $\delta \in [0, 0.025]$.

Using the AWD tool, we plot the asymptotic weight distribution curves of AR3A-JSCC code, AR4JA-JSCC code, $\mathbf{B}_{sp_opt1}$, $\mathbf{B}_{sp_opt2}$, and $\mathbf{B}_{sp_opt3}$, in Fig. 12. As seen in the figure, AR4JA-JSCC code and $\mathbf{B}_{sp_opt3}$ have TMDRs while AR3A-JSCC code, $\mathbf{B}_{sp_opt1}$ and $\mathbf{B}_{sp_opt2}$ do not have TMDRs. The TMDR values of AR4JA-JSCC code and $\mathbf{B}_{sp_opt3}$ are around 0.017 and 0.003, respectively. A larger TMDR value implies a lower error-floor. When a P-LDPC code does not possess a TMDR value, its error-floor performance is hard to be predicted and can only be found out by simulations.

2) Generic protomatrix of size 4×7 *and* $p_1 = 0.04$*:* Next, we increase the generic protomatrix size to 4×7 and use the FSTCT method to search for protomatrices under Benchmarks B_1 and B_2 separately. Since the protomatrix size is not small, we apply the DE searching approach. The parameters G, S and p_c in the DE algorithm are set to 800, 800 and 0.88, respectively. With Benchmarks B_1 and B_2, the FSTCT method finds protomatrices shown in (29) and (30), respectively.

$$\mathbf{B}^{47}_{sp_opt1} = \begin{pmatrix} 1 & 0 & 0 & 1 & 2 & 0 & 1 \\ 0 & 1 & 1 & 1 & 2 & 1 & 0 \\ 0 & 2 & 1 & 3 & 0 & 2 & 0 \\ 1 & 0 & 0 & 2 & 0 & 0 & 0 \end{pmatrix} \tag{29}$$

$$\mathbf{B}^{47}_{sp_opt2} = \begin{pmatrix} 0 & 0 & 0 & 2 & 2 & 0 & 1 \\ 1 & 0 & 0 & 2 & 0 & 0 & 0 \\ 1 & 2 & 0 & 3 & 1 & 1 & 0 \\ 0 & 1 & 3 & 1 & 1 & 2 & 0 \end{pmatrix} \tag{30}$$

The source and channel thresholds of $\mathbf{B}^{47}_{sp_opt1}$ and $\mathbf{B}^{47}_{sp_opt2}$ are shown in Table III and Table II, respectively. Both source thresholds are higher than those of the AR3A-JSCC and AR4JA-JSCC codes. Moreover, $\mathbf{B}^{47}_{sp_opt1}$ has a lower channel threshold than AR3A-JSCC while $\mathbf{B}^{47}_{sp_opt2}$ has a lower channel threshold than AR4JA-JSCC. Using the AWD tool, we further find that $\mathbf{B}^{47}_{sp_opt1}$ has no TMDR and $\mathbf{B}^{47}_{sp_opt2}$ has a TMDR of around 0.007.

TABLE IV
CHANNEL THRESHOLDS OF THE GENERIC PROTOMATRICES AT DIFFERENT p_1 VALUES. THE BEST CHANNEL THRESHOLD AT EACH p_1 IS IN BOLD FONT WHILE THE WORST ONE IS IN BLUE COLOR.

p_1	Shannon limit	AR3A-JSCC	AR4JA-JSCC	$\mathbf{B}_{sp_opt1}$	$\mathbf{B}_{sp_opt2}$	$\mathbf{B}_{sp_opt3}$	$\mathbf{B}_{sp_opt4}$
0.04	-7.00 dB	-5.918	-5.767	$\mathbf{-6.102}$	-5.810	-5.782	-4.459
0.08	-4.19 dB	$\mathbf{-3.414}$	-3.188	-3.171	-3.027	-3.198	-2.647
0.12	-2.44 dB	$\mathbf{-1.680}$	-1.409	-1.151	-1.228	-1.366	-1.239
0.16	-1.13 dB	-0.094	0.522	0.57	0.193	0.227	$\mathbf{-0.185}$
0.20	-0.00 dB	2.073	3.553	2.30	1.381	2.055	$\mathbf{0.816}$

TABLE V
THE SOURCE THRESHOLDS AND CHANNEL THRESHOLDS OF THE OPTIMIZED DOUBLE PROTOGRAPHS IN [33] WHEN $p_1 = 0.04$. THE SIZE OF EACH DOUBLE-PROTOGRAPH IS 5×9. THE SHANNON LIMIT IS -7.00 dB

	$\mathbf{B}_J^{opt_1}$	$\mathbf{B}_J^{opt_2}$	$\mathbf{B}_J^{opt_3}$	$\mathbf{B}_J^{opt_4}$
p_{1_th}	0.082	0.082	0.144	0.136
$(E_s/N_0)^*$ (dB)	-5.130	-5.398	-5.267	-5.571

3) Generic protomatrix of size 3×5 *and* $p_1 = 0.16$*:* We design a generic protograph with a size of 3×5 for a relatively large p_1, i.e. $p_1 = 0.16$. We use the source threshold and channel threshold of AR3A-JSCC at $p_1 = 0.16$ as the benchmark. Referring to Tables III and IV, we set Benchmark B_3: ($\bar{p}_1 = 0.228$, $(E_s/N_0)' = -0.094$ dB). By using the FSTCT joint optimization method and the brute force searching approach, we obtain

$$\mathbf{B}_{sp_opt4} = \begin{pmatrix} 0 & 1 & 1 & 1 & 2 \\ 1 & 1 & 1 & 0 & 1 \\ 0 & 1 & 2 & 2 & 0 \end{pmatrix}. \tag{31}$$

with a source threshold of 0.324 and a channel threshold of -0.185 dB at $p_1 = 0.16$. However, $\mathbf{B}_{sp_opt4}$ has no TMDR.

4) Comparison of channel thresholds at different p_1 *values:* For the six 3×5 protomatrices discussed above, namely AR3A-JSCC, AR4JA-JSCC, and $\mathbf{B}_{sp_opt1}$ to $\mathbf{B}_{sp_opt4}$, we derive their channel thresholds at different p_1 values using the PEXIT-JSCC algorithm and list them in Table IV. We can see that among all codes, $\mathbf{B}_{sp_opt1}$ has the lowest channel threshold (-6.102 dB) when $p_1 = 0.04$; AR3A-JSCC has the lowest channel thresholds (-3.414 dB and -1.680 dB, respectively) when $p_1 = 0.08$ and 0.12; $\mathbf{B}_{sp_opt4}$ has the lowest channel thresholds (-0.185 dB and 0.816 dB, respectively) when $p_1 = 0.16$ and 0.20. As shown in Table IV, these lowest channel thresholds are within 1 dB from the Shannon limits. Moreover, the six 3×5 protomatrices have different decoding-threshold rankings at different p_1 values. The results indicate that a generic protograph optimized at a given p_1 does not guarantee the best performance at other p_1 values.

5) Comparison of thresholds with those of DP-JSCCs: Table V shows the source thresholds and channel thresholds of the optimized double protographs in [33] (denoted by $\mathbf{B}_J^{opt_1}$ to $\mathbf{B}_J^{opt_4}$) when $p_1 = 0.04$. Comparing the results with those in Table II and Table III indicate that our constructed P-JSSCs can achieve better thresholds than $\mathbf{B}_J^{opt_1}$ to $\mathbf{B}_J^{opt_4}$.

B. Error Performance

In addition to theoretical analysis, computer simulations are performed. The encoding and decoding processes have been described in Sect. II-A and Sect. II-B, respectively. We denote the number of source symbols in a frame by $N_s = n_r z$ and set

the maximum number of decoding iterations to $I_{\max} = 200$. Three types of error rates are recorded.

- Source symbol error rate (SSER) is evaluated by comparing the original source symbols with the recovered source symbols.
- Transmitted bit error rate (TBER) is evaluated by comparing the code bits sent through the channel with the corresponding recovered bits.
- Frame error rate (FER) is evaluated by comparing the original JSCC codeword with the recovered codeword.

The error rate results are recorded if (i) the number of frames simulated exceeds 10^5, or (ii) the number of error frames exceeds 50 and the number of frames simulated is no smaller than 5000.

Fig. 13 plots the SSER performance of all our constructed protographs optimized at $p_1 = 0.04$. We also plot the results of AR3A-JSCC, AR4JA-JSCC and the optimized double protographs in [33] (i.e., $\mathbf{B}_J^{opt_1}$ to $\mathbf{B}_J^{opt_4}$) for comparison. From Fig. 13(a) where N_s is around 12800, we can observe that

1) $\mathbf{B}_{sp_opt1}$ and $\mathbf{B}_{sp_opt1}^{47}$ outperform AR3A-JSCC in both the waterfall and high-SNR regions while all three codes have error floors;
2) $\mathbf{B}_{sp_opt2}$, $\mathbf{B}_{sp_opt3}$ and $\mathbf{B}_{sp_opt2}^{47}$ have, respectively, 0.20 dB, 0.25 dB and 0.25 dB gains over AR4JA-JSCC at a BER of 10^{-6}
3) $\mathbf{B}_{sp_opt3}$ and $\mathbf{B}_{sp_opt2}^{47}$ has no error floor down to a BER of 10^{-6};
4) optimized double protographs $\mathbf{B}_J^{opt_2}$ and $\mathbf{B}_J^{opt_4}$ in [33] are outperformed by all the generic protographs in the waterfall region and they do not have error floors down to a BER of 10^{-6};
5) error floors exist or start to emerge for AR3A-JSCC, $\mathbf{B}_{sp_opt1}$, $\mathbf{B}_{sp_opt2}$ and $\mathbf{B}_{sp_opt1}^{47}$ which do not have TMDRs.

When N_s is reduced to around 3200, we can observe from Fig. 13(b) that the performance of these codes are degraded. Yet, $\mathbf{B}_{sp_opt1}$, $\mathbf{B}_{sp_opt2}$ and $\mathbf{B}_{sp_opt2}^{47}$ still outperform the optimized double protographs $\mathbf{B}_J^{opt_1}$ and $\mathbf{B}_J^{opt_3}$ in [33] down to a BER of around 10^{-6}.

Fig. 14 depicts the SSER and TBER performance of $\mathbf{B}_{sp_opt1}$, $\mathbf{B}_{sp_opt2}$, $\mathbf{B}_{sp_opt3}$, $\mathbf{B}_{sp_opt4}$, AR3A-JSCC code, AR4JA-JSCC code when $N_s = 12800$ and $p_1 = 0.04, 0.08, 0.12, 0.16$ and 0.20. We can observe that the error performance of all codes degrades in general as p_1 increases from 0.04 to 0.20. It is because the initial LLR information of the source symbols decreases as p_1 increases. Hence in order to achieve the same error performance, a larger E_s/N_0 is required to compensate the reduction in initial information as p_1 increases.

Referring to Fig. 14(a) where $p_1 = 0.04$, the initial LLR information of the source symbols is relatively large compared with the channel LLR information of the transmitted bits. The source symbols therefore have a higher chance of being decoded correctly even when the transmitted bits are decoded wrongly. Thus SSER is better (lower) than TBER for the same E_s/N_0 in the given SNR range. As p_1 increases, the initial LLR information of the source symbols decreases. The source symbols rely more heavily on the channel LLRs of the transmitted bits for correct decoding. When the transmitted bits cannot be decoded correctly and hence cannot pass reliable information to the source symbols, the source symbols become even less likely to be decoded correctly. Therefore when $p_1 = 0.20$, Fig. 14(e) shows that SSER is worse (higher) than TBER for the same E_s/N_0 in the given SNR range. Based on the same arguments, we can also conclude the following.

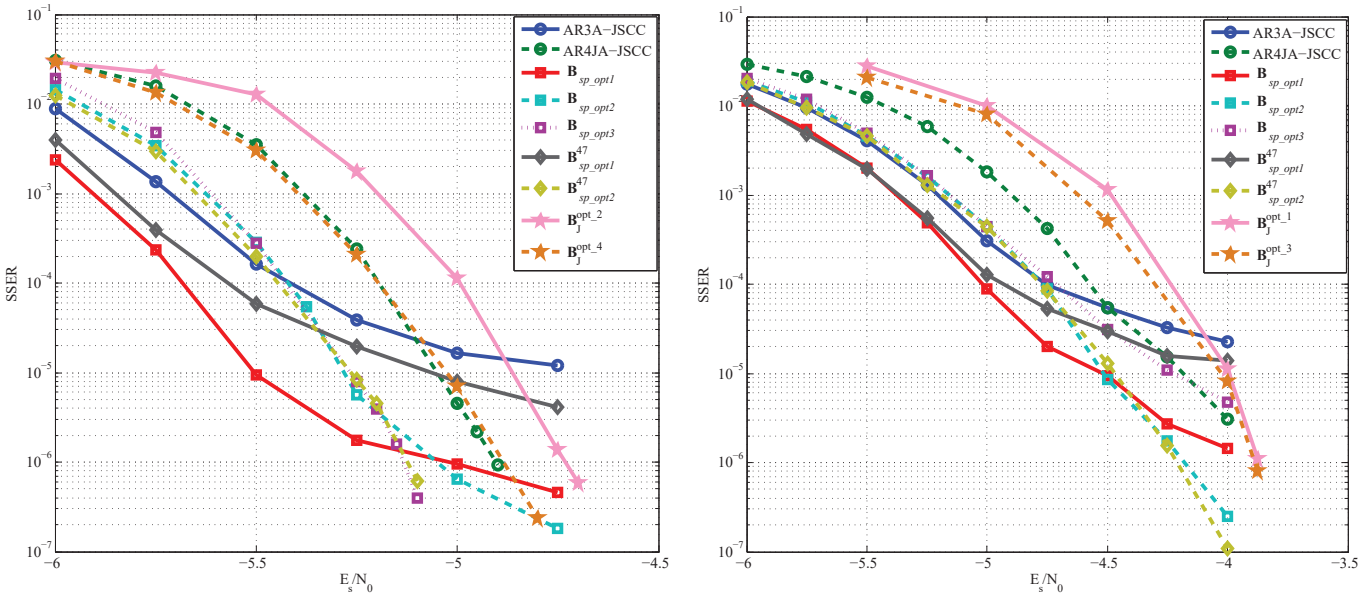


Fig. 13. SSER performance comparison at $p_1 = 0.04$. (a) $N_s = 12800$ (i.e. $z = 6400$) for all generic 3×5 protographs, and $N_s = 12864$ (i.e. $z = 4288$) for all generic 4×7 protographs. Starting from $E_s/N_0 = -5.0$ dB, -5.25 dB, -5.0 dB and -5.2 dB, respectively, the numbers of error frames of AR4JA-JSCC, $\mathbf{B}_{sp_opt3}$, $\mathbf{B}^{47}_{sp_opt1}$ and $\mathbf{B}^{47}_{sp_opt2}$ recorded are below 50. (b) $N_s = 3200$ (i.e. $z = 1600$) for all generic 3×5 protographs, and $N_s = 3264$ (i.e. $z = 1088$) for all generic 4×7 protographs. Starting from $E_s/N_0 = -4.25$ dB, -4.25 dB, -4.5 dB and -4.25 dB, respectively, the numbers of error frames of AR4JA-JSCC, $\mathbf{B}_{sp_opt2}$, $\mathbf{B}_{sp_opt3}$ and $\mathbf{B}^{47}_{sp_opt2}$ recorded are below 50.

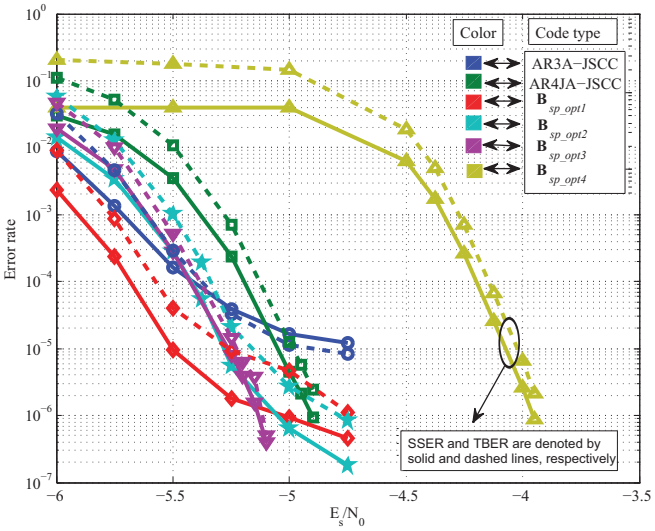
- When p_1 is low (e.g., 0.04), the source symbols have a higher chance of being decoded correctly but the lack of TMDRs of the codes causes an error floor (see Table II and the error curves for AR3A-JSCC, $\mathbf{B}_{sp_opt1}$ and $\mathbf{B}_{sp_opt2}$ in Fig. 14(a)).
- When p_1 becomes large (e.g., 0.20) and approaches the source thresholds of the codes (e.g., AR3A-JSCC and AR4JA-JSCC have source thresholds of 0.228 and 0.212, respectively), the low initial LLR information of the source symbols cannot ensure successful decoding of the symbols even at high SNR, causing error floors to occur (see the error curves for AR3A-JSCC and AR4JA-JSCC in Fig. 14(e)).

Moreover, at the waterfall region, we can observe

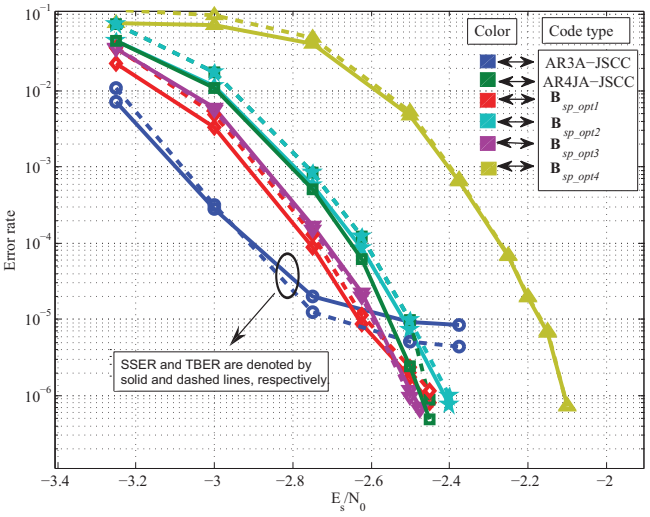
1) at $p_1 = 0.04$, $\mathbf{B}_{sp_opt1}$ performs the best while $\mathbf{B}_{sp_opt4}$ performs the worst;
2) at $p_1 = 0.08$, AR3A-JSCC performs the best while $\mathbf{B}_{sp_opt4}$ performs the worst;
3) at $p_1 = 0.12$, AR3A-JSCC performs the best while $\mathbf{B}_{sp_opt1}$ performs the worst;
4) at $p_1 = 0.16$, $\mathbf{B}_{sp_opt4}$ performs the best while $\mathbf{B}_{sp_opt1}$ performs the worst; and
5) at $p_1 = 0.20$, $\mathbf{B}_{sp_opt4}$ performs the best while AR4JA-JSCC performs the worst;

The relative error performances of the codes therefore match with the channel thresholds listed in Table IV.

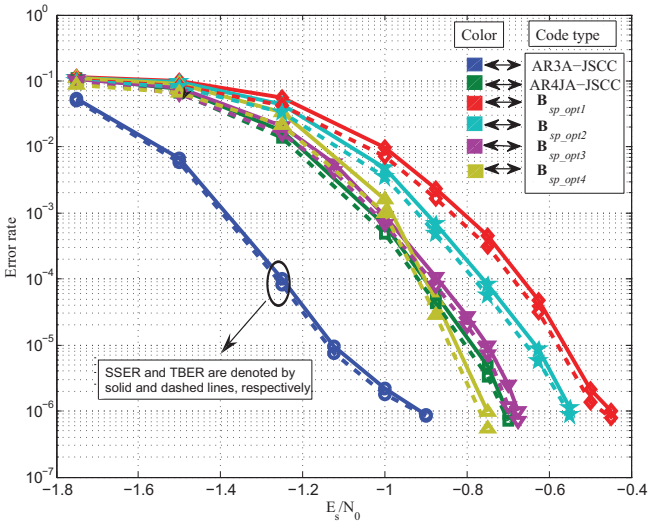
Fig. 15 depicts the frame error rate (FER) performance of $\mathbf{B}_{sp_opt1}$, $\mathbf{B}_{sp_opt2}$, $\mathbf{B}_{sp_opt3}$, $\mathbf{B}_{sp_opt4}$, AR3A-JSCC code, AR4JA-JSCC code when $N_s = 12800$ and $p_1 = 0.04, 0.08, 0.12, 0.16$ and 0.20. The characteristics of the curves can be explained similarly using the aforementioned arguments.



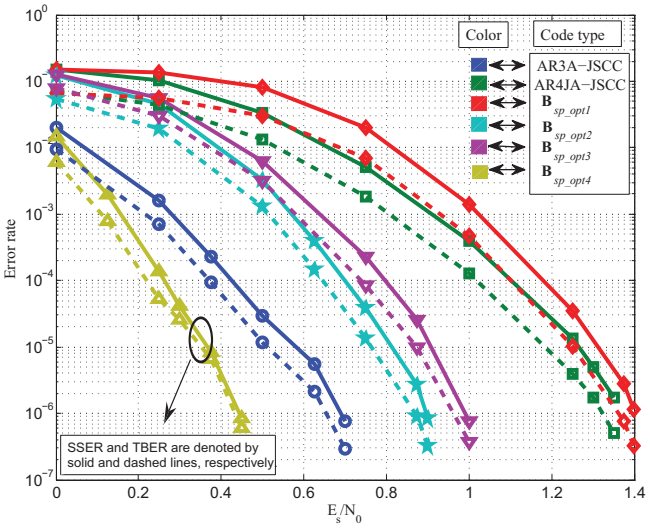
(a) $p_1 = 0.04$



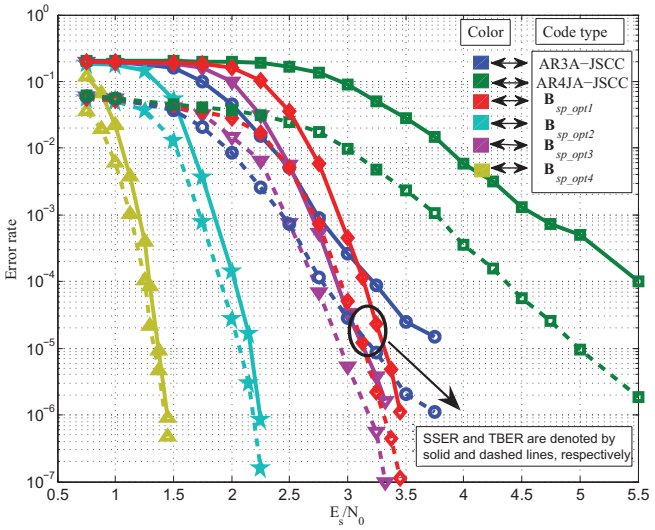
(b) $p_1 = 0.08$



(c) $p_1 = 0.12$



(d) $p_1 = 0.16$

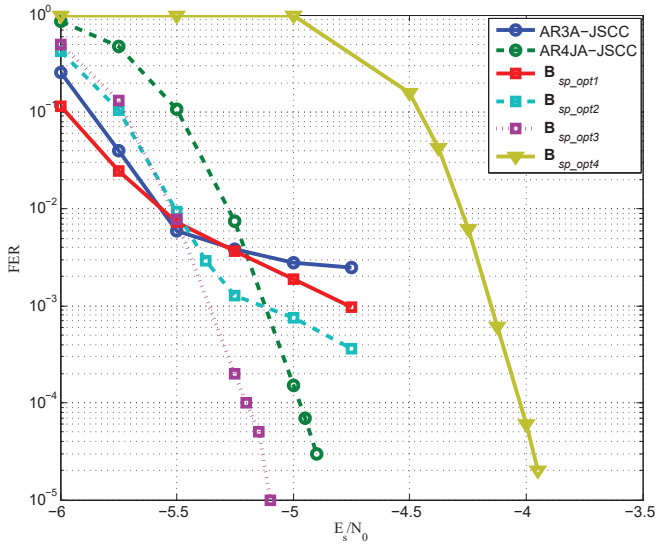


(e) $p_1 = 0.2$

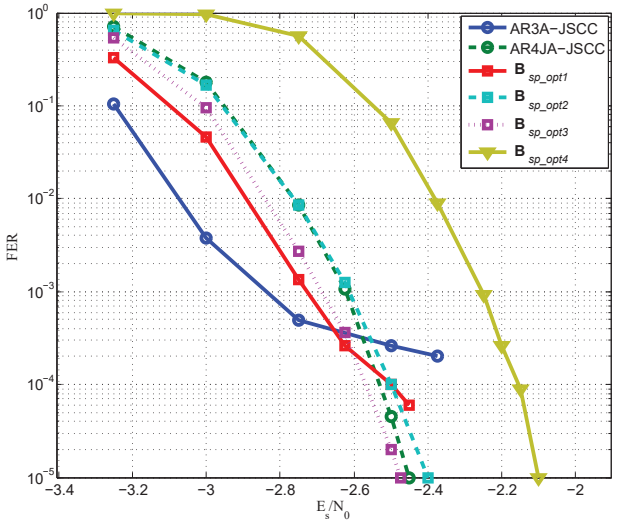
p_1	The E_s/N_0 value of the point, starting from which the error frames does not reach 50. (dB)					
	AR3A-JSCC	AR4JA-JSCC	$\mathbf{B}_{sp_opt1}$	$\mathbf{B}_{sp_opt2}$	$\mathbf{B}_{sp_opt3}$	$\mathbf{B}_{sp_opt4}$
0.04	None	−5.00	None	None	−5.25	−4.00
0.08	None	−2.50	−2.625	−2.50	−2.625	−2.20
0.12	−1.125	−0.875	−0.625	−0.625	−0.80	−0.75
0.16	0.50	1.25	0.75	0.75	0.875	0.30
0.20	3.25	None	3.25	2.15	3.00	1.375

(f) The table lists the starting E_s/N_0 values, from which the numbers of error frames recorded are below 50.

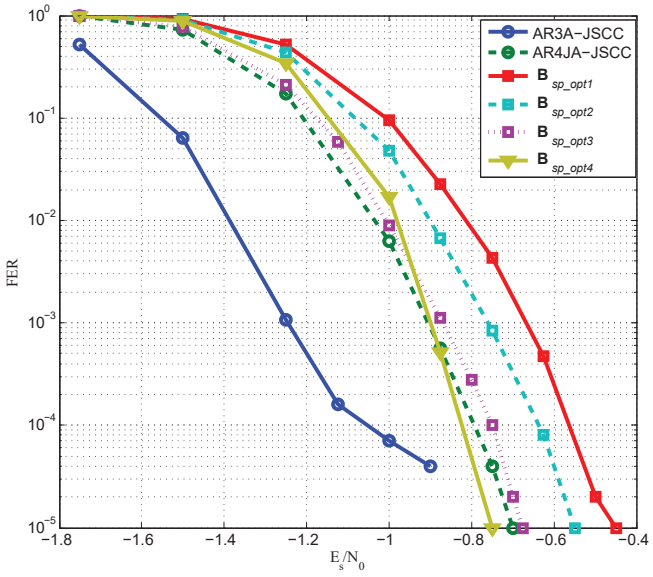
Fig. 14. Source symbol error rate (SSER denoted by solid lines) and transmitted bit error rate (TBER denoted by dashed lines) performance of AR3A-JSCC, AR4JA-JSCC and the optimized codes constructed ($\mathbf{B}_{sp_opt1}$ to $\mathbf{B}_{sp_opt4}$). $N_s = 12800$. The source thresholds of AR3A-JSCC, AR4JA-JSCC, $\mathbf{B}_{sp_opt1}$, $\mathbf{B}_{sp_opt2}$, $\mathbf{B}_{sp_opt3}$ and $\mathbf{B}_{sp_opt4}$ are 0.228, 0.212, 0.25, 0.275, 0.242 and 0.324, respectively.



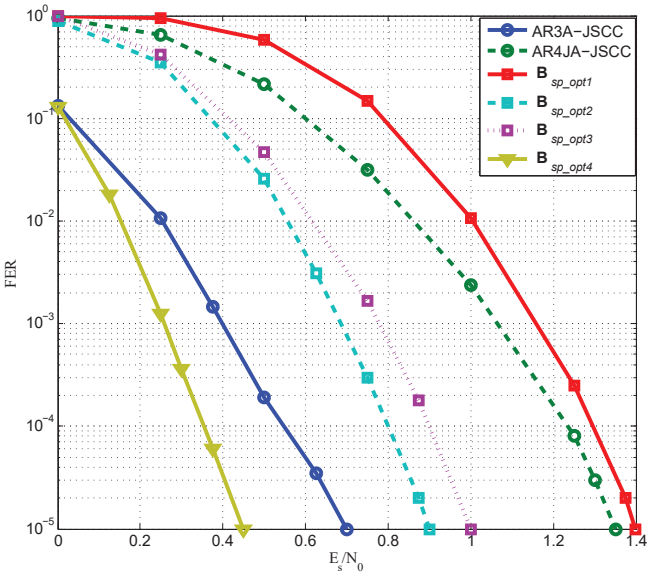
(a) $p_1 = 0.04$



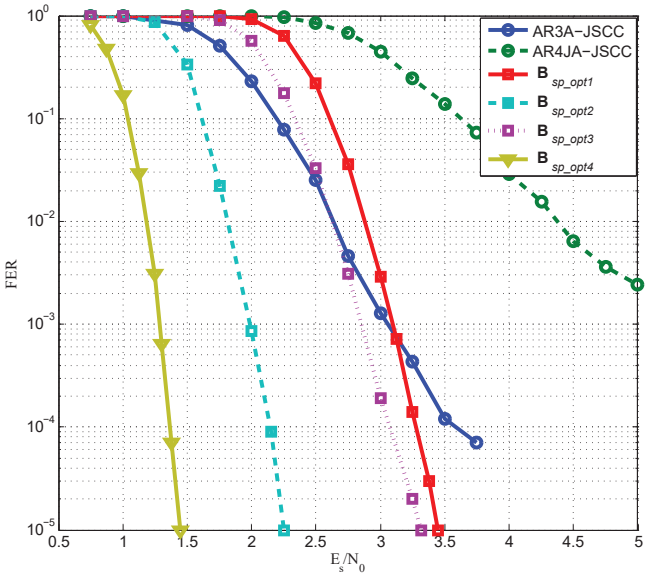
(b) $p_1 = 0.08$



(c) $p_1 = 0.12$



(d) $p_1 = 0.16$



(e) $p_1 = 0.20$

Fig. 15. Frame error rate (FER) performance of AR3A-JSCC, AR4JA-JSCC and the optimized codes constructed ($\mathbf{B}_{sp_opt1}$ to $\mathbf{B}_{sp_opt4}$). $N_s = 12800$. The source thresholds of AR3A-JSCC, AR4JA-JSCC, $\mathbf{B}_{sp_opt1}$, $\mathbf{B}_{sp_opt2}$, $\mathbf{B}_{sp_opt3}$ and $\mathbf{B}_{sp_opt4}$ are 0.228, 0.212, 0.25, 0.275, 0.242 and 0.324, respectively.

IV. Conclusions

In this paper, we propose a JSCC system based on a generic protograph, namely protograph-based JSCC (P-JSCC). We present a PEXIT-JSCC algorithm to evaluate the channel threshold and propose a source generic protograph EXIT (SGP-EXIT) algorithm to evaluate the source threshold of a P-JSCC. Based on the PEXIT-JSCC and SGP-EXIT algorithms, we further propose a joint optimization method to design P-JSCCs (i.e., generic protographs) with good channel and source thresholds. In terms of theoretical thresholds and error rates, the performance of the P-JSCCs constructed by the joint optimization method are found to outperform JSCCs based on double protographs.

We further find that the source symbol error rate (SSER) is better (lower) than the transmitted bit error rate (TBER) when the probability of "1" in the source sequence p_1 is small, and vice versa. Moreover, error floors are caused by (i) a lack of TMDRs in the protographs when p_1 is small, and (ii) small initial LLR information of the source symbols when p_1 is large and approaches the source thresholds.

References

[1] F. C. M. Lau and J. Zhan, "Joint source-channel codes based on a single protograph," in *2021 11th International Symposium on Topics in Coding (ISTC)*, 2021, pp. 1–5.

[2] C. E. Shannon, "A mathematical theory of communication," *Bell Syst. Tech. J.*, vol. 27, no. 3, pp. 379–423, Oct. 1948.

[3] R. J. McElience, *The theory of information and coding*. Cambridge University Press, 1977.

[4] K. Sayood and J. C. Borkenhagen, "Use of residual redundancy in the design of joint source/channel coders," *IEEE Trans. Commun.*, vol. 39, no. 6, pp. 838–846, June. 1991.

[5] J. Hagenauer, "Source-controlled channel decoding," *IEEE Trans. Commun.*, vol. 43, no. 9, pp. 2449–2457, Sep. 1995.

[6] M. Jeanne, J. C. Carlach, and P. Siohan, "Joint source-channel decoding of variable-length codes for convolutional codes and turbo codes," *IEEE Trans. Commun.*, vol. 53, no. 1, pp. 10–15, 2005.

[7] P. Burlina and F. Alajaji, "An error resilient scheme for image transmission over noisy channels with memory," *IEEE Trans. Image Process.*, vol. 7, no. 4, pp. 593–600, Apr. 1998.

[8] C. Y. Bi and J. Liang, "Joint source-channel coding of JPEG 2000 image transmission over two-way multi-relay networks," *IEEE Trans. Image Process.*, vol. 26, no. 7, pp. 3594–3608, Jul. 2017.

[9] M. Van Der Schaar, "Adaptive cross-layer protection strategies for robust scalable video transmission over 802.11 wlans," *IEEE JSAC.*, vol. 21, no. 10, pp. 1752–1763, Dec. 2003.

[10] M. G. Martini, M. Mazzotti, C. Lamy-Bergot, J. Huusko, and P. Amon, "Content adaptive network aware joint optimization of wireless video transmission," *IEEE Commun. Mag*, vol. 45, no. 1, pp. 84–90, Jan. 2007.

[11] A. Zribi, R. Pyndiah, S. Zaibi, F. Guilloud, and A. Bouallegue, "Low-complexity soft decoding of Huffman codes and iterative joint source channel decoding," *IEEE Trans. Commun.*, vol. 60, no. 6, pp. 1669–1679, June. 2012.

[12] D. J. C. MacKay and R. M. Neal, "Near Shannon limit performance of low-density parity-check codes," *Electron. Lett.*, vol. 32, no. 18, pp. 1645–1646, 1996.

[13] T. J. Richardson and R. L. Urbanke, "The capacity of low-density parity-check codes under message-passing decoding," *IEEE Trans. Inf. Theory*, vol. 47, no. 2, pp. 599–618, Feb. 2001.

[14] S. ten Brink, G. Kramer, and A. Ashikhmin, "Design of low-density parity-check codes for modulation and detection," *IEEE Trans. Commun.*, vol. 52, no. 4, pp. 670–678, Apr. 2004.

[15] M. Fresia, F. Perez-Cruz, and H. V. Poor, "Optimized concatenated LDPC codes for joint source-channel coding," in *Proc. ISIT*. IEEE, June. 2009, pp. 2131–2135.

[16] M. Fresia, F. Perez-Cruz, H. V. Poor, and S. Verdú, "Joint source and channel coding," *IEEE Signal Process. Mag.*, vol. 27, no. 6, pp. 104–113, Nov. 2010.

[17] D. Divsalar, C. Jones, S. Dolinar, and J. Thorpe, "Protograph based LDPC codes with minimum distance linearly growing with block size," in *IEEE Global Telecomm. Conf.*, St. Louis, 2005, pp. 1152–1156.

[18] A. Abbasfar, D. Divsalar, and K. Yao, "Accumulate repeat accumulate codes," *IEEE Trans. Commun.*, vol. 55, no. 4, pp. 692–702, 2007.

[19] D. Divsalar, S. Dolinar, C. Jones, and K. Andrews, "Capacity approaching protograph codes," *IEEE J. Sel. Areas Commun.*, vol. 27, no. 6, pp. 876–888, Aug. 2009.

[20] Y. Fang, G. Bi, Y. L. Guan, and F. C. M. Lau, "A survey on protograph LDPC codes and their applications," *IEEE Commun. Surveys Tuts.*, vol. 17, no. 4, pp. 1989–2016, 4th Quart., 2015.

[21] J. G. He, L. Wang, and P. Chen, "A joint source and channel coding scheme base on simple protograph structured codes," in *Proc. Int. Symp. Commun. Inform. Tech.*, Gold Coast, Australia, Oct. 2012, pp. 65–69.

[22] L. Wang, L. Xu, and S. H. Hong, "New results on radiography image transmission with unequal error protection using protograph double LDPC codes," in *Proc. Int. Symp. on Medical Information and Communication Technology (ISMICT)*, Firenze, April 2014, pp. 1–4.

[23] J. G. He, Y. Li, and G. F. Wu, "Performance improvement of joint source-channel coding with unequal power allocation," *IEEE Wireless Commun. Lett.*, vol. 6, no. 5, pp. 582–585, 2017.

[24] C. Chen, L. Wang, and S. Liu, "The design of protograph LDPC codes as source codes in a JSCC system," *IEEE Commun. Lett.*, vol. 22, no. 4, pp. 672–675, Apr. 2018.

[25] Q. Chen, L. Wang, S. Hong, and Z. Xiong, "Performance improvement of JSCC scheme through redesigning channel code," *IEEE Commun. Lett.*, vol. 20, no. 6, pp. 1088–1091, Jun. 2016.

[26] C. Chen, L. Wang, and F. C. M. Lau, "Joint optimization of protograph LDPC code pair for joint source and channel coding," *IEEE Trans. Commun.*, vol. 66, no. 8, pp. 3255–3267, Aug. 2018.

[27] Q. Chen, L. Wang, S. Hong, and Y. Chen, "Integrated design of JSCC scheme based on double protograph LDPC codes system," *IEEE Commun. Lett.*, vol. 23, no. 2, pp. 218–221, Feb. 2019.

[28] H. V. B. Neto and W. Henkel, "Multi-edge optimization of low-density parity-check codes for joint source-channel coding," in *Proc. 9th Int. ITG Conf. Syst., Commun. Coding (SCC)*, Munich, Germany, Jan. 2013, pp. 1–6.

[29] S. Hong, Q. Chen, and L. Wang, "Performance analysis and optimization for edge connection of JSCC system based on double protograph LDPC codes," *IET Commun.*, vol. 12, no. 2, pp. 214–219, Jan. 2018.

[30] Q. Chen, F. C. M. Lau, H. Wu, and C. Chen, "Analysis and improvement of error-floor performance for JSCC scheme based on double protograph LDPC codes," *IEEE Trans. Veh. Technol.*, vol. 69, no. 12, pp. 14 316–14 329, Dec. 2020.

[31] Q. Chen, S. Hong, and Y. Chen, "Design of linking matrix in JSCC scheme based on double protograph LDPC codes," *IEEE Access*, vol. 7, pp. 92 176–92 183, July. 2019.

[32] S. Liu, C. Chen, L. Wang, and S. Hong, "Edge connection optimization for JSCC system based on DP-LDPC codes," *IEEE Wireless Commun. Lett*, vol. 8, no. 4, pp. 996–999, Aug. 2019.

[33] S. Liu, L. Wang, J. Chen, and S. Hong, "Joint component design for the JSCC system based on DP-LDPC codes," *IEEE Trans. Commun.*, vol. 68, no. 9, pp. 5808–5818, June 2020.

[34] C. Chen, L. Wang, and Z. Xiong, "Matching criterion between source statistics and source coding rate," *IEEE Commun. Lett.*, vol. 19, no. 9, pp. 1504–1507, Sep. 2015.

[35] D. Divsalar, "Ensemble weight enumerators for protograph LDPC codes," in *IEEE Int. Symp. Inf. Theory*, Seattle, Washington, USA, 2006, pp. 1554–1558.

[36] X. Y. Hu, E. Eleftheriou, and D. M. Arnold, "Regular and irregular progressive edge-growth Tanner graphs," *IEEE Trans. Inf. Theory*, vol. 51, no. 1, pp. 386–398, Jan. 2005.

[37] S. ten Brink, "Convergence behavior of iteratively decoded parallel concatenated codes," *IEEE Trans. Commun.*, vol. 49, no. 10, pp. 1727–1737, Oct. 2001.